Development of High Loading Lithium Sulfur Battery

by

Matthew Li

A thesis

presented to the University of Waterloo

in fulfillment of the

thesis requirement for the degree of

Master of Applied Science

in

Chemical Engineering

Waterloo, Ontario, Canada, 2016

Author’s Declaration

I hereby declare that I am the sole author of this thesis. This is a true copy of the thesis, including any required final revisions, as accepted by my examiners.

I understand that my thesis may be made electronically available to the public

Abstract

The topic of batteries has been given much attention. With the development and rapid improvement of transistors, the power requirement of our electronics are quickly becoming higher and higher. Unlike Moore's law, since the commercialization of its newest iteration, the lithium ion battery (LIB) the battery technology has shown only incremental improvement. Popular fashionable companies such as Tesla has developed electric vehicles with acceptable mileage of around 400 km per change. Even with Elon Musk's ambitious goals, championing the change in the whole automotive industry, scientific barriers are met as the theoretical limits of the battery materials are reached. To answer to this, researchers around the globe have revisited old and thought to be too difficult to implement technologies such as the lithium sulfur battery (LIS). A LIS possesses a sulfur cathode and a lithium anode, which leads to one key advantage to LIBs, sulfur can store/bond to lithium at much higher ratios than traditional cathodes in LIBs. Boasting a theoretical energy density of about 5 times that of the current LIB, this technology has the potential to ultimately surpass and replace a lot of the LIB out in the market. Unfortunately, the reason it was given up decades ago was due to its debilitating problems. First and foremost, sulfur is a very good insulator making it difficult to efficiently deliver electrons to its reaction sites. Furthermore, during discharge and charge sulfur will dissolve into the electrolyte, upon deposition on insulating spots in the cell it disconnects itself from the circuit. In short the LIS are not durable and suffers from terrible cycle life. To address these challenges, researchers have develop many clever engineering designs such as modification to the electrodes, electrolyte, separator, anode all of which have shown great promise on the lab scale resulting in LIS with impressive performance surpassing LIBs. The first part of this thesis will be to develop a type of nitrogen doped porous carbon material that will serve as a modifier for the

cathode improving its performance over bare sulfur cathodes. A first discharge of 1060 mAh g^{-1} was achieved at 0.2C and stabilized to ~860 mAh g^{-1} , a ~81 % retention in capacity over 100cycles. This material also offered significant improvements in rate performance. It was able to discharge at 5C delivering ~600 mAh g^{-1}. Both the cycle stability and rate performance illustrates the impact of using nitrogen doping for LIS.

In order for LIS to reach the market the one key parameter has to be addressed first and that is the loading of sulfur in the battery. Many of publications have displayed near theoretical/ideal performances, seemingly revolutionizing the battery industry, but unfortunately at impractically low loadings. Continuing from the low loading high performance electrodes of the first part of this thesis, the work in the second part will improve upon the porous carbon material allowing its application in high loading electrodes. It was quickly discovered that the nano-sized nitrogen doped porous carbon was unable to yield a robust electrode at higher loadings. Cracks and pinholes formed throughout the electrode leading to the eventual flaking/delamination of material. Larger nitrogen-doped porous carbon was synthesized through a simple addition of NaCl into the synthesis procedure. This aggregated the smaller polymer particles together forming micron size particles. Larger nitrogen doped porous carbon easily formed thick electrodes while at the same time achieved exceptional electrochemical performance. With a discharge rate of 0.1C a specific capacity of 1300 mAh g^{-1} was reached stabilizing to 1050 mAh g^{-1} after 50 cycles. Moreover, at 0.2C and 0.5C discharge rates this material delivered ~1000 mAh g^{-1} and 900 mAh g^{-1} respectively on first discharge.

Acknowledgements

The work reported herein was financially supported by the National Science and Engineering Research Council of Canada, Waterloo Institute for Nanotechnology, and the University of Waterloo.

The author would like to thank Dr. Zhongwei Chen, and Dr. Aiping Yu for their helpful guidance and tremendous assistance in the Master's study. A special thanks to Dr. Yining Zhang for working closely with me and providing me with direction, valuable advice and support.

Many thanks go to author's colleagues including, Xiaolei Wang, Kun Feng, Fathy Hassan, Hadis Zarrin, Ge Li, Moon Gyu Park, , Ja-Yeon Choi, Ariful Hoque, Siamak Ghorbani, Yun-seok Jun, Jared Lenos, Dongun Lee, Gaopeng Jiang, Rasim Batmaz, Abdul Rahman Ghannoum, Abel Sy, Gregory Lui, Guihua Liu, Min Ho Seo, Pouyan Zamani, Salah Abureden, Zhiyu Mao, Jing Fu, Lucas Lim, Lathankan Rasemthiram, Ricky Tjandra, Pei Yu, Terry Yan, Hao Liu, Xiaogang Fu, Jing Zhang, Pan Xu, Calvin Xu, and many other friends for their assistance and support.

I would also like to thank my parents, Kei Li and Jenny Li for their consistent love and support for me.

Moreover I would like to acknowledge support from my reviewers, including Professor Zhongwei Chen, Professor Michael Fowler, and Professor Mark Pritzker.

Table of Contents

List of Figures

List of Tables

List of Abbreviations, Symbols and Nomenclature

LIBs	Lithium ion batteries
SEM	Scanning Electron Microscopy
TEM	Transmission Electron Microscopy
XRD	X-ray Diffraction
TGA	Thermal Gravimetric Analysis
CNT	Carbon nanotube
BET	Brunauer–Emmett–Teller
EIS	Electrochemical impedance spectroscopy
DOL	1,3 dioxolane
DME	dimethoxyethane
KB	Ketjen black 600 JD
NPC	nitrogen doped porous carbon
LIS	lithium sulfur battery
PS	polysulfide
MF	melamine formaldehyde resin
EV	electric vehicle

1.0 Introduction

Batteries are a part of the lives of almost everyone on Earth. From electric vehicles to novelty items such as smartwatches, the applications are endless. Many modern day battery technologies fall into the category of lithium-ion batteries (LIB). Although large improvements from its predecessors have been made the limitation of LIBs are quickly approaching. As of 2016, many automotive companies are trying to develop commercially viable electric/ hybrid vehicles. In response to climate change concerns, electric vehicles (EVs) or hybrids as green alternative to internal combustion engines in hopes of relieving some of humanity's dependency on fossil fuels. Interestingly, the use of electricity is actually releases more greenhouse gas than burning fossil fuels in some regions in the world such as California and Singapore. This is because the method of which electricity is produced in those regions uses very greenhouse gas heavy methods such as coal or even the greener natural gas. Hence, the total emission of an electric vehicle is not simply related to its tailpipe but a look at the whole process to obtain the energy is required. Although this is true, in most regions of the world nuclear and hydro does serve as a significant source of green electricity and provide justification of the use of electric vehicles. Unfortunately, many other problems still exists. These include the economic concerns to purchase an electric vehicle and concerns regarding the driving range. Because consumers are afraid to take electric vehicles on longer drives due to fear of running out of power (range anxiety), the application of electric cars has been limited to mostly city driving. Tesla, a well-known electric vehicle company has by far the longest lasting battery pack, boasting a range of about 450 km (depending on the model) on a full charge. With an initial entry into the luxurious car market, Tesla has recently announced it will take orders for its mass produced and quite affordable $35,000 USD Model 3, possibly breaking into a much larger and impactful consumer market. Concerns also exists for creating the necessary battery-charging infrastructure to alleviate some of the range anxiety. Tesla has committed itself to create fast charging stations reasonably spaced throughout the United States of America and even placed in overseas countries such as China. It is important to realize

that a boost in infrastructural support for EVs is only half of the problem at hand. The other problem is that the batteries currently being used in EVs do not have high enough energy density to compete with internal combustion engines. In other words, they are required to be recharged/refueled much sooner than regular cars.

Longer lasting batteries are desperately needed in modern society to not only provide relatively trivial conveniences in our life such as cell phones but to ensure that we can effectively combat global warming by phasing out combustion engines. This thesis will discuss the operating mechanism and limitations of a modern lithium ion battery. To follow will be a section dedicated to lithium sulfur batteries (LIS) including advantages, challenges and common strategies to compact those challenges. LIS research is a hot topic nowadays for many groups across the globe. This thesis will discuss in more detail the mechanism of one specific type of solution to the problems of LIS followed by criticism of the practicality of the work published thus far and introducing a novel solution.

1.1 Lithium Ion Batteries

Batteries have been a device used by mankind to store energy for many centuries. The earliest form of a battery could be dated back to a 2000-year old clay jar with copper cylinders with iron rods found in Baghdad. Cells nowadays come in two different types, primary and secondary. Secondary batteries are rechargeable whereas the primary cells are not. This ability of the secondary battery is due to the reversible nature of the redox reactions that occurs. The first secondary battery was the lead-acid battery developed by Planté in the year of 1859. Over the years many other technologies have emerged such as NiMH and gained substantial popularity. Others, such as NiCd battery have been phased out due to its negative effects on the environment. Newer and more current electronics such as smartphones, laptops, tablets and even electric vehicles all contains what is known as the 3V lithium-ion battery (LIB). Being more compact and lightweight, the LIBs have grown to be a major portion of the battery market [1].

1.1.1 Principle of operation

A lithium ion battery (LIB) as all electrochemical systems consists of a cathode and an anode. Commercially available LIBs consists of lithium metal oxide cathodes such as for example $LiCoO_2$ or $LiFePO_4$ and a carbon based material for the anode. Both of these operate under the principles of lithium intercalation. This technology dates back to the 1970s in a conference proceeding in *Fast Ion Transport in Solids* by Steel and Armand [2]. The mechanism of energy storage in lithium ion batteries (LIB) lies in the lithium-ions being transferred from the anode and intercalated into the layered lattice structure of the cathode material. Intercalation can occur in two different forms depending of the type of metal oxide. In the case of a spinel metal oxide, either a single-phase mechanism occurs or a two-phase reaction. The single phase entails a unit cell expands and contracts during lithiation and delithiation respectively. As for the two-phase system, the ratios between these phases changes upon lithiation. There are different type of metal oxides that dictates the avenue of which the Li^+ is allowed to enter its lattice. For example, the three-dimensional spinel structure of $LiMnO_2$ typically have better mass transfer properties than a two-dimensional layered metal oxide cathode such as $LiCoO_2$. During operation, Li^+ moves from a high chemical potential (anode) to a lower chemical potentials (cathode) during discharge. The voltage of discharge is also of concerns because it controls the degree of lithiation in the metal oxide, possibly stressing the crystal lattice irreversibly if not controlled properly. This would lead to quick battery cycle degradation. Throughout the Li^+ transfer process, electrons transfers from the anode to the cathode converting the difference in chemical potential into electrical power. After delivering the power to the electric load (vehicle, cell phone), to recharge, an external voltage is applied to induce The transfer of the Li^+ from the low chemical potential cathode back to the higher chemical potential to recharge the battery. The cathode in commercial LIBs are usually lithium metal oxides, while the anode is a carbon based material. Additionally, an electrically insulating and Li^+-permeable membrane separates the cathode from the anode. This membrane or so-called separator is crucial to ensure that the electron actually transfers through the external circuit and does not undergo short-circuiting. While at the same time, this membrane cannot be too thick/heavy to reduce its impact on the specific and volumetric energy density.

Furthermore, the medium through which Li^+ is conducted is usually an organic-based electrolyte, which has low viscosity and high Li^+ mobility at room temperature. If the mobility of Li^+ is low the battery will prematurely reach its cycle cut off voltage resulting in lost capacity. Typical salts used in the electrolyte includes $LiPF_6$ for LIBs and LiTFSI for lithium sulfur batteries. Most important of all, the electrolyte must be stable in a relatively wide voltage window, and operating temperature to decrease the chance for a catastrophic failure of the cell.

To fabricate a LIB, a slurry has to be formulated and then casted onto an aluminum (for cathode) or copper (for anode). A crucial component of the slurry is the conductive additive. Because the metal oxide is not very electronically conductive, it requires the use of conductive additive such as various carbon black. Furthermore, to obtain a mechanically stable electrode, the use of a binder is required. Typically, this binder is made of various different polymers such as sodium carboxyl methylcellulose and polyvinylidene fluoride. The binder is required to have good surface interaction to adhere all both the active material and the conductive additive together in addition to the current collector. The thickness and solid content of the slurry is of great important when controlling the mass loader of the binder. Finally, the manner in which the electrode is dried will affect its porosity, typically the atmosphere, temperature and convection rate is optimized to obtain a certain desired electrode quality.

1.2 Limitation of current LIB

Current LIB technology has several disadvantages ranging from slow recharge and discharge rates to its temperature sensitivity. The most important parameter enabling for its application in so many devices is its energy density. How much energy the LIB can store on a given charge and, how long is required to recharge an electronic device reduces to a matter of the energy density of the battery. Unfortunately, the energy density of current LIB material is reaching its theoretical limit. Meaning that minimal change in energy density can be expected in the future if the same metal oxide anode and carbon are used for the cathode and anode, respectively. To put this into perspective, the theoretical practical energy density taking into account all the cell components is ~250 Wh kg^{-1} [3, 4]. The state of the art LIBs have an

energy density of 210 Wh kg^{-1} [3]. From rough calculations, a mere 20% further improvement can be made. This limitation stems from the inherent ability of the metal oxide and graphite to uptake and accommodate Li^+ into its crystal lattice. As the chemical formula of $LiCoO_2$ suggests, only one lithium cation is bonds to one cobalt oxide anion. A simple calculation based on molar masses indicates that at least 13 grams of deadweight metal oxide material exist for every gram of lithium in the battery. The lithium only represents 7% of the total mass of the cathode. A more convenient representation would be to measure how much charge or specific capacity the cathode material can take, typically expressed in mAh g^{-1} to align with popular convention. The lithiation of the cobalt oxide cathode material theoretically has a specific capacity of 274mAh g^{-1} but practically only ~150 mAh g^{-1} [5]. The key to improving the energy density relies on our ability to find hosts for lithium, forming compounds that must possess higher lithium to deadweight host material ratio. One possible candidate of cathode material is sulfur. When paired with a lithium anode this type of technology is called a lithium-sulfur battery (LIS).

1.3 Lithium sulfur battery

Incorporation of sulfur as a cathode material has been sought after as far back as the 1970s [6]. The operation of a LIS is fundamentally different from a modern day intercalation chemistry based LIB. In a LIS the sulfur is dissolved into the electrolyte during discharge upon reduction from its $S_{8(S)}$ form to polysulfides S_8^{-2}. A LIB, as stated previously, relies on a simple entry of Li^+ into the lattice of the metal oxide crystal structure. Furthermore, the reduction mechanism of sulfur is much more complex in nature compared to that of metal oxides. The following equations illustrate a proposed reduction pathway:

$$S_8 + 2e^- \leftrightarrow S_6^{2-} + \frac{1}{4}S_8$$

$$S_6^{2-} \leftrightarrow 2S_3^{-}$$

$$4S_3^{-} + 2e^- \leftrightarrow 3S_4^{-2}$$

$$S_4^{-2} + 6e^- \leftrightarrow 4S^{2-}$$

Overall:

$$S_8 + 16Li^+ + 16e^- \rightarrow 8Li_2S$$

Equation 1: Discharge Mechanism of Sulfur in a LIS [7]

Similar to the LIB, the charge carriers are Li^+, exchanged back and forth between the cathode and the anode. In this case the product formed when discharged is lithium sulfide (Li_2S), possessing a much higher lithium to dead weight material than CoO_2. As a matter of fact, the specific capacity of sulfur for lithium is actually ~1675 mAh g^{-1} [8]more than 5.6 times that of CoO_2. Although specific capacity is a useful unit of measure of the duration of a discharge cycle, an electrical device requires energy which relates to the voltage of the battery. In terms of energy density (Wh kg^{-1}) sulfur possesses 2500 Wh kg^{-1} if an lithium anode is used in a full cell. After all the other components of the battery such as current collector, separator and electrolyte are taken into consideration, the practical energy density is more along the lines of 700 Wh kg^{-1} , whereas commercially available LIB has only realized 210 Wh kg^{-1} [3]. In short, the LIS can potentially offer more than a 3-fold increase in energy density, quite the revolutionary increase, if successful. Please refer to Appendix A for detailed calculation on specific capacity and energy density.

Sulfur exists at room temperature in its orthorhombic octet solid form. It is insoluble in typical organic electrolyte (1,3 dioxolane and dimethoxyethane). Upon accepting an electron, sulfur is reduced to S_8^{2-} (soluble) which is then further reduced to S_6^{2-}(soluble). It is speculated that the S_6^{2-} spontaneously forms $S_3^{\cdot-}$ (soluble) third-order polysulfide radicals. These radicals are further reduced to S_4^{2-} (soluble) and finally to S^{2-} which is insoluble. Note the reactant to the discharge/reduction and final product of a LIS are insoluble in the electrolyte. This implies that the cell undergoes some form of "electro-stripping" and electrodeposition over the course of a single discharge. Upon charge the insoluble Li_2S are dissolved and redeposited as sulfur at the end of the cycle. Unfortunately, LIS technology has yet to be used in mainstream electronic devices due to many technical challenges centred on the complex discharge/charge

mechanism of sulfur. These challenges resulted in poor cycle stability and poor practical capacity from sulfur nullifying all of its benefits.

1.3.1 Technical challenges

The challenges of LIS can be described by three main points. The first and relatively least important is the 80% volumetric expansion of sulfur after lithiation. This is problematic because the volume expansion can lead to disconnection of lithiated sulfur (Li_2S) from the circuit. Furthermore, a volumetric expansion would possibly lead to the overall macroscopic expansion of the whole battery packing problems. Publications addressing this issue are rare and if it is discussed, it is usually not the key point of the paper [9]. This expansion is not so much a concern at this point of the LIS research field because most sulfur cathode already have a lot of void space built into its architecture. This void space is not necessary created for the purpose of mitigating the effects of volumetric expansion but instead are created to allow more electrolyte to contact the sulfur, which leads to the discussion of the next two problems. The next two problems are significantly more detrimental to performance than the first. The second problem stems from the fact that sulfur is a very good electrical insulator, much better than its metal oxide cathode counterparts. This would commonly require some sort of conductive additive in the electrode to efficiently deliver electrons to the sulfur. Conductive additives are not uncommon and are actually found in all LIBs. Metal oxides found in commercially available cathodes are indeed not as insulating as sulfur but they are also not conductive as well. It is naïve to believe a simple addition of conductive additive into a sulfur cathode would resolve the problem as it did for the metal oxide cathodes. The insulating nature of sulfur would not be as large as a challenge if the following problem did not exist. The third problem is the dissolution of sulfur into the electrolyte during discharge. This works synergistically with the conductivity problem. The dissolution/deposition of sulfur and Li_2S upon cycling leads to the possibility of undesired redistribution of sulfur among its conductive matrix. This usually creates large agglomerates of sulfur throughout the battery. Regardless of what is used as a conductive additive, it has to be homogenously dispersed within the cathode and maintain intimate contact with all of the sulfur. If sulfur

is redistributed and agglomerated during cycling, the homogeneity and intimacy of electrical contact would be compromised. The result, large agglomerations of sulfur particles, of which, only the surface is electrochemically active leaving the core completely unusable. Adding to this, the dissolution of sulfur into the electrolyte changes the fundamental mechanism of the reaction. No longer are the Li^+ simply entering and positioning itself in a crystal lattice structure of metal oxides but the reduction and oxidation mechanism of LIS becomes a full fledged surface reaction. Reactions sites are dictated by not only the availability of Li^+ and electrons (in the case of metal oxides) but also on the availability of solvated polysulfide anions (PS). In other words, the mass transfer of PS becomes a concern. Transfer of PS to the reaction sites is not the aforementioned concern, instead, because the rate of reduction (kinetics of PS reduction) is inherently controlled by the use defined discharge rate, the possibility of mass transfer of PS away from the reaction sites becomes a major concern. Hence, the overarching consequences of the dissolution of sulfur is the possibility of diffusion of soluble PS species out of the cathode and its subsequent consumption by unwanted side reactions. The first set of side reactions are the disproportionation of PS at different oxidation states and results in precipitates of solid S_8 in electronically inaccessible locations in the battery. The second set of reactions occur at the lithium anode. Once the PS escapes the cathode it can also further diffuse to the surface of anode and directly complete a redox reaction on the anode circumventing the electron transfer across the external circuit. Simply put, PS can short circuit on the lithium anode resulting in poor capacity. Moreover, the products of these short circuit reactions are usually Li_2S or Li_2S_2 both of which are sparingly soluble in typical LIS electrolyte. This indicates that any PS that is short circuited on the anode will remain electrochemically inactive on the anode throughout the lifespan of the battery because there is no mechanism of which it can be brought back to the cathode. In a sense, sulfur disconnects itself from the circuit/battery over a few cycles and results in a quick decrease in battery capacity. Finally, the last problem is a low coulumbic efficiency. Because higher order PS can be short circuited/reduced directly on the lithium anode, it opposes the act of recharging. Specifically, during charging, higher PS are generated at the cathode. For example, sulfur at its -2 oxidation state is oxidized to -1, -2/3, -2/4, -2/6, -2/8 and then finally to 0 upon full charge. This

complex oxidation reaction mechanism entails some mass transfer complications. Again, not mass transfer limitations but opportunity for PS escaping into the bulk electrolyte. Once the initial soluble -2/4 or S_4^{2-} species are generated/charged from S_3^{2-} at the cathode they will be allowed to diffuse to the anode (shuttle effect), discharging themselves once in contact with the anode and reduce/discharge back to its -2/3 or S_3^{2-} oxidation state. This re-discharged S_3^{2-} will have to be recharged once again at the cathode. The redundant nature of charging a LIS is reflected in its the coulumbic efficiency of LIS, creating cells which delivers significantly less amount of electrical energy than that was "stored" in them. Typical LIB cells have far above 99% coulombic efficiency, indicating for every 100 electrons that was stored in the battery, 99 can be extracted. In the case of LIS, without any effective mitigation strategy a coulombic efficiency of as low of 70% will be obtained. A 70% efficient battery will increase the greenhouse gas generated to charge the battery stripping EVs of its single most important benefit.

1.3.2 Literature review of application of porous carbon for LiS

LIS has many problems: poor practical capacity, poor cycle durability and low coulombic efficiency. All of these problems have to be addressed before any commercialization of LIS can be made. Although known since the 1970s, research into LIS have been halted until recently. Many groups around the globe have began to furiously solve these three problems since 2009. The pioneering work of Xiulei Ji, Kyu Tae lee and Linda Nazar has brought forward the use of porous carbon. After impregnation of sulfur into the pores, the wall of these pores can serve both as a conductive matrix while the complex pore network can increase the diffusion resistance of PS [10]. Ji *et al* has successfully prevented major S redistribution, PS shuttle and allow for much more reversible LIS cells. Boasting an initial discharge capacity of 1000 mAh g^{-1} (60% of theoretical)and remained relatively stable for 20 cycles. There is much room for improvements if LIS is to be taken seriously as a successor to LIBs. Since then, many concepts have been tested to overcome the problems with the LIS battery. These concepts typically fall into one of three categories, modification of the separator [11, 12], electrolyte [13, 14] and electrode material design. Modification of separator involves the application of Li^+ selective film that halts any PS diffusion.

Typical examples involves, graphene, porous carbon and Nafion coatings on the separator. Additive is used in electrolyte to limit the dissolution of sulfur. For example, researchers attempted to add PS into the electrolyte and due to the common-ion effect, the dissolution of new sulfur is hindered. Obviously, this is not a complete solution, as the PS additive would decrease the overall energy density of the cell. Researchers have also used ionic liquid as the electrolyte. The so-called tailor made solvents can be made such that PSs are insoluble, Li^+ is sufficiently high while at the same time remain stable in the operating voltage of the cell. Modification of the cathode material usually incorporates the use of some porous network to house the sulfur. A high porosity, high surface area material is usually used to allow efficient delivery of electrons to the sulfur. Furthermore, this sulfur housing also usually have some mechanism of which can limit the PS diffusion out of the cathode. Recently, electrode material designs incorporated the use of graphene foams [15, 16] , carbon nanotubes [17] and various types of porous carbon[18, 19] as conductive S housing. In attempts to mitigate the effects of the PS shuttle, researchers aim to increase tortuosity of the diffusion pathway with complex pore structures. Additionally, various other chemical species (metal oxide, atomically doped carbon, polar functional groups) have been introduced into the to attract and retain PS [16, 20, 21]. The use of materials such as nitrogen-doped graphene is also another popular area of research. Cycle stability have improved to the point where 1500 cycles can be achieved in the laboratory with capacities well over 70% theoretical achievable.

Despite all of this work, minimal work has been performed to obtain commercially feasible electrodes. One important metric for practicality is the energy density, which directly relates to the sulfur loading. Recently Pope et al published an informative review [22], that describes the relationship between sulfur loading per area and battery energy density. This review states that most LIS studies have reported energy densities that are not even comparable to current LIB. Regardless of the business strategy to enter the market, a marginally better product is usually a hard sell for a factory to risk an alteration in manufacturing processes. Nearly 8 years after the ground breaking work of Ji et al [10], recent work published recently still mainly focusses on the material at 1-2 mg cm^{-2} [22] rather than aiming for

practicality. This could be due to a few reasons, first it could be difficult to achieve a higher loading and some studies have also shown an associated decrease in performance at higher loading [23, 24]. Some notable work has recently been done by Donghai's group [21, 25, 26]that has achieved very high sulfur loading electrodes up to 5 mg cm^{-2}. The performance of LIS has no doubt dramatically improved in the lab setting throughout the years, but a practical electrode is still a long way off. The objective of this thesis is to tackle this specific problem and provide some much needed insight on how to obtain higher loading sulfur electrodes.

1.4 Particle size

Before discussion of strategies to achieve high loading, the effect of particle size on performance must be explained. The use of nanoparticle conductive additives have been well studied in the field of LIS. A high surface area allows for a highly uniform distribution of sulfur and maximizes the effective capacity of the cell. Furthermore, although carbon nanoparticles such as Ketjen Black are not porous, they can hinder PS diffusion when stacked together in a confined space forming interparticle pores. The use of nanoparticles has obvious advantages and is indeed commonly a theme of many publications in the LIS field [27, 28]. Unfortunately, nanoparticles do not allow high loading electrodes to be achieved. Even at sulfur mass loadings as low as 3 mg cm^{-2}, the mechanical properties of electrode starts to compromise. During drying of the electrode, surface tension caused by the small interparticle pores stresses the whole electrode and generate cracks and deformations [23, 29] . This is not a problem for a lab-scale test as sampled electrodes areas can be handpicked without much consequences. In the case of a full-scale manufacturing line, quality control would be a huge problem [23]. A natural method to solve this problem would be to use a higher binder content. A binder is a component in the slurry that acts as an adhesive for all the components of the slurry in addition to adhering the electrode to its current collector. A higher binder content would yield a better film quality and can potentially alleviate the cracking problem. However, the use of more binder comes at the cost of two very important parameters. Firstly, because this reduced the mass loading of sulfur in the slurry, a higher electrode thickness is required. In others words, it artificially

creates a bulkier battery. The second compromised parameter is the porosity of the electrode. A nanoparticle network would create very small interparticle pores. Although this slows PS diffusion, it also hinders Li^+ diffusion and increases the internal diffusion resistance of the cell drastically. In certain cases, a majority of the sulfur will never be reached by the lithium ions. This will result in higher loading electrodes but effectively the capacity will be much lower than even that of low loading electrodes. This phenomenon is an example of a low effectiveness factor for the electrode. Effectiveness factor (η) is defined as the ratio between average reaction rate when diffusion is taken in to account over pure bulk phase reaction rate. η is strongly related to the Thiele modulus. The Thiele modulus is a dimensionless number that represents the ratio of reaction rate to the diffusion rate. A higher Thiele modulus results in a lower effectiveness factor, although, the exact relationship is dependent on the exact geometry of the system. Therefore, the problem at hand for the second parameter is to create a thick electrode while maintaining a high effectiveness factor/low Thiele modulus. Fortunately, this is not a new problem in the field of chemical engineering and has been narrowed down to decreasing diffusion length, reaction rate or increasing diffusion coefficient or pore size. Of all these possibilities the only practical ones are to either increase the diffusion coefficient or increase the pore size. Methods to improve the diffusion coefficient will not be considered here, but instead this thesis will focus on increasing pore size. Increasing pore size is an interesting topic because it is seemingly contradictory to limiting PS diffusion out of the cathode. Proposed by Xiao *et al* [24], a large particle composed of nanoparticles can be used to solve this problem. By creating micron sized particle composed of nanoparticle Xiao *et al* has demonstrate relatively functional electrode at loading up to 4mg cm^{-2}. This so-called hierarchical architecture of material can trap sulfur with inter-nanoparticle pores within each micron particle while increasing porosity for Li^+ diffusion for the bulk of the electrode. Low porosity within each particle but high porosity for overall electrode. This thesis will be adding to this work, exploring a different material synthesis route. Through the modification of surface charge, nanoparticle polymers/silica composites can be agglomerated forming large micron-sized particles.

1.5 Project scope and objectives

The aim of this project will be to develop a strategy to increase the loading of sulfur without sacrificing too much of its performance. In terms of scope, all experiments will be conducted at a proof-of-concept level without any scale up tests. The key to the design is to modify surface charge to induce agglomeration and form micron sized particles composed of nanoparticles i.e., a hierarchical structure. Electrochemical performance tests will be done *via* a coin cell to demonstrate the validity of this concept and electrode design.

The objectives are stated below:

1. First develop a porous carbon material that is able to effectively combat against the challenges of LIS
2. Develop this technology further to enable high loading electrodes

2.0 Physical and electrochemical characterization methods

Physical and electrochemical characterization of the various material and LIS cells are important tools to allow me to quantitatively compare samples. Physical characterization techniques such as dynamic light scattering, electrophoresis, scanning electron microscopy, transmission electron microscopy, BET surface area and pore volume analysis, X-ray diffraction, thermogravimetric analysis and ultraviolet-visible spectroscopy are all used to determine specific traits of the materials. Electrochemical techniques such as galvanostatic discharge is used to emulate actual battery operating conditions allowing us to determine whether the quality of the created LIS. Furthermore, other electrochemical technique such as electrochemical impedance spectroscopy can offer valuable insight into the nature of mass transfer in a cell. This is especially important when investigating high loading electrodes where diffusion of ions and electron conductance become a major problem. To follow is a brief description of each characterization methods used in the research presented in this thesis.

2.1 Scanning electron microscopy

Scanning electron microscopy (SEM) utilizes electrons beams to analyze the topological properties of a sample. Fired from an electron gun, the beam is passed through a condenser and focusing lens composed of electromagnetic fields. Once the beam makes contact with the sample a combination of three events occur. The electron can be reflected, absorbed and cause excitation of the electrons within the material. After measuring all of these signals with detectors, a signal is sent to the computer which creates a real time image displaying the morphology of the sample. Typical SEMs operate under high vacuum (~10-5 mbar), although SEMs that can operate under low vacuum and even with different atmospheres exists. These are called atmospheric SEMs. In this thesis, SEM will be used to examine the pore structure of the porous carbon in addition to obtaining a visual confirmation of their respective particle sizes. A Zeiss Leo FESEM 1530 scanning electron microscope (SEM) is used to characterize the morphology of the material.

SEM will be used in this thesis to characterize the surface morphology of nitrogen-doped porous carbon and also provide visual confirmation of their particle sizes. The pore size should be ~20 nm and can visually inspected with SEM. Upon enlargement of particle size, SEM will be also used as evidence to illustrate this shift in particle size distribution. The sample with the NaCl addition is expected to be significantly larger than that of the sample without NaCl.

2.2 X-ray diffraction

X-ray diffraction is a technique that is used to characterize the crystal structure of samples. The basic concept is that electromagnetic waves such as X-rays, can be diffracted by the crystal structure to form an interference pattern. The intensities of these patterns can be detected and correlated to structure and order of the atoms are in the sample. Bragg's law is used to relate the scattering angle to the lattice spacing and is given in the following widely known equation:

$$2d\ sin\theta = n\lambda$$

Equation 2: Bragg's Law

where d is the lattice spacing, θ is the incident angle of the X-ray, n is any whole integer and λ is the wavelength of the X-rays. The left figure below depicts the experimental setup while the right one illustrates the relationship between the lattice spacing and scattering angle geometricaly.

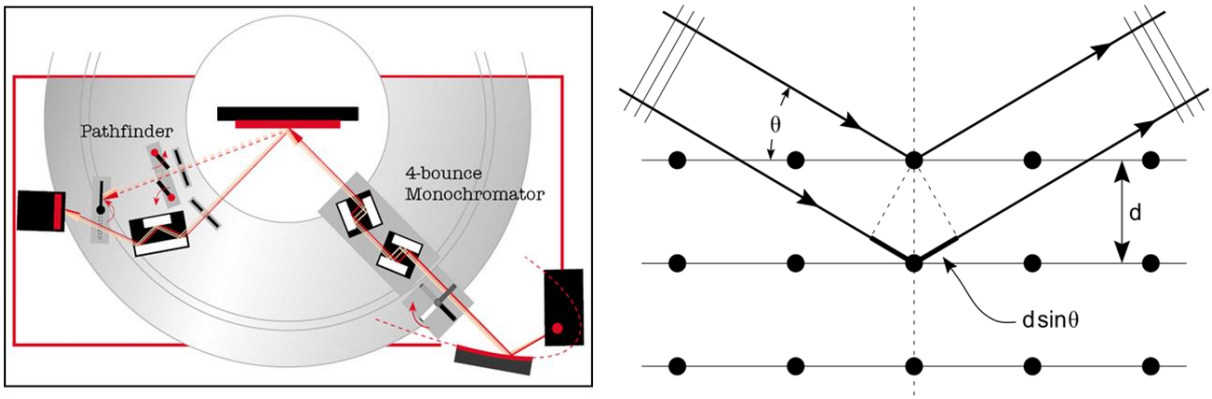

Figure1: Illustration of XRD operation

Furthermore, a smaller grain size leads to in a broader peak whereas a narrow peak would indicate a large sulfur grains. The grain size is computed with the Scherrer equation:

$$T = \frac{K\lambda}{\beta cos\theta}$$

Equation 3: Scherrer Equation

where T is the mean size of the order domains, K is a dimensionless shape factor, β is the width of the peak at half the maximum intensity of the peak, θ is the peak location, and λ is the X-ray wavelength. XRD measurements are performed on a MiniFlex 600 Rigaku unit.

XRD will also be used to show the successful removal of silica template after HF etching. It is expected that the amorphous broad silica peak (2θ =~20º) disappear after HF etching. While slight peaks at ~42º and ~27º should be present representing the (100) and (002) plane of graphite respectively. After sulfur infiltration, there should also be a new broad peak at 25 º. Also XRD is used to analyze the grain size of sulfur in the porous carbon. The purpose is to provide evidence of a thin film of sulfur as appose to sulfur agglomerates which is to be expected due to the high surface area and pore volume of the nitrogen doped porous carbon.

2.3 Thermogravimetric analysis

Thermogravimetric analysis (TGA) is a technique where the weight change of a sample is measured as a function of temperature. Samples can also be exposed to different atmospheres as they are being heated during TGA. For example, heating carbon in nitrogen gas does not result in any weight loss even at 900 Celsius but once the atmosphere is changed to air, carbon is readily burned away. A typical TGA measures the sample weight with a precise balance while purging the heated region with the desired type of gas. The heating is done in a small furnace and the temperature is precisely measured with a temperature resistance probe in close vicinity to the sample holder. The sample holder is usually made up of an inert heat resistant material such as platinum and alumina. A platinum sample holder is used in this research study.

The main purpose of TGA in this work is to determine the exact sulfur amount in the porous carbon/sulfur composite. Sulfur boils at ~444 Celsius so a sharp decline in mass is to be expected near this temperature. If the atmosphere was chosen to be nitrogen, all the sulfur would evaporate leaving behind the porous carbon when this temperature is reached. The mass changed measured by the TGA will determine the accurate composition of the porous carbon/sulfur composite. This is imperative to obtain an accurate estimate of specific capacity. TGA was performed in this thesis on a TA instrument Q500. The final mass remaining for the NPC/S70 should be ~30% of the original because ~70% of the original composite is sulfur.

2.4 X-ray photoelectron spectroscopy

X-ray photoelectron spectroscopy (XPS) is a method that provides information of the electronic structure of atoms and ionization energy of certain electrons of those elements. X-rays are bombarded at the sample and the resulting electrons ejected are captured by detectors. The basic concept XPS revolves around the conservation of energy. Since the wavelength of the X-ray is known prior to hitting the sample, the energy entering the system is known. Upon interaction with the atoms of the sample, electrons will be ejected from the sample with a certain amount of kinetic energy through the photoelectric effect. An

energy balance is performed to determine how much energy is absorbed by the atom. This absorbed energy is called the binding energy or the ionization energy of the atom. This provide valuable information of the orbitals from which these electrons are emitted and the nature of the chemical bonds. Furthermore, because different electron shells require drastically different ionization energies, electron configuration of the sample can be found and hence a fingerprint for the atom in the sample. XPS is also surface sensitive and can only penetrate modestly into the sample.

XPS will be used in this thesis to find, quantify the degree and type of nitrogen doping. The three type of nitrogen doping should be pyridinic, pyrrolic, and graphitic. The amount of nitrogen doping is should be more than 5% by mass due to the high nitrogen content in the melamine carbon precursor.

2.5 Dynamic light scattering

Dynamic light scattering (DLS) is a technique used to determine the particle size distribution of particle suspended in a solvent. The main principle of operation is to direct a laser beam (monochromatic and coherent electromagnetic wave) at the sample. If the particle sizes is on the order of the wavelength, it will scatter the light and create interference patterns on the detector. This is repeated very quickly, taking many interference patterns over time because the particles fluctuate in position due to Brownian motion. Brownian motion is random but it is also strongly related to the viscosity, temperature and most importantly the size of the particles. Therefore, if temperature and viscosity is kept constant, the degree of variation of the DLS intensity signal can be related to the particle size. To quantify the degree of variation, typically an autocorrelation function is used. An autocorrelation relates the difference in two signals to the time difference between those two measurements. The hydrodynamic particle size can be obtained by fitting the autocorrelation function. This method is used to confirm the differences in hydrodynamic particle size. Because no surfactants or polymer stabilizers are used, the hydrodynamic particle size should be similar to the real particle size.

In this thesis, DLS is performed at 25 ^{o}C using a Corbouan DLS 135 Particle Size Analyzer with a 65 mW monochromatic red laser (λ = 658 nm). DLS measurements will be used to confirm the particle size increase after NaCl addition and provide information on the particle size distribution.

2.6 Zeta Potential Analyzer

Zeta potential analysis (ZPA) which is derived from electrophoretic light scattering is a technique used to determine the surface charge of a particle. Two electrode are immersed in the suspension of interest. A voltage between two electrodes is applied to induce movement of the any charged particles. The electrophoretic mobility is measured and then the following equation is used to deduce the zeta potential.

$$U_E = 2\varepsilon Z \frac{f(Ka)}{3n}$$

Equation 4: Equation used to deduce zeta potential

where U_E is the measured electrophoretic mobility, ε is the dielectric constant, Z is the zeta potential f(Ka) is Henry's function and n is the viscosity of the solvent. Because the viscosity of the solution is known and the particle size can be detected simultaneously, it is possible to back calculate the electrostatic attraction is on the surface of the particles. This yields the surface charged/zeta potential of the particles. This method is used to quantify the surface charge of the polymer particles with and without surface charge modifiers. These measurements are done through electrophoresis with a WALLIS Zeta Potential from Cordouan in this thesis.

Zeta potential measurements will be used to indicate the degree of surface charge change after addition of NaCl. Of which will be ultimately used to support the proposed synthesis mechanism. It is expected that the sample without NaCl will possess a higher negative surface charge. Whereas the sample with NaCl will have a near 0 mV surface charge.

2.7 Potentiostatic Electrochemical impedance spectroscopy

Potentiostatic electrochemical impedance spectroscopy (EIS) is a very useful technique in the field of electrochemical engineering. It can provide insight into the mechanism of an electrochemical cell. EIS operates by treating the cell as a circuit of capacitors and resistors, the configuration of which is decided by the user. By applying an AC voltage signal at different frequencies over a pre-set voltage range a corresponding alternating current (AC) can be obtained. The dependence of the impedance of an AC circuit on the frequency can be used to fit a proposed electric circuit model. This method has been used to investigate the change in impedance with respect to an increase in particle size. In the case of lithium sulfur battery the circuit below has been used [30]. Re is the ohmic loss from the electrolyte resistance, Rint/CPEint is the resistance between the conductive interface of sulfur and any conductive material, Rct/CPEdl is the charge transfer resistance interpreted as the charge transfer process at the interface between the electron conductor and electrolyte, and CPEdiff is the lithium ion diffusion resistance [30-32]. Through fitting the model (impedance versus frequency function) to the data set obtained from experiments a value for each circuit element can be obtained. Mass transfer difference between samples can then be discussed based on magnitude of each circuit element.

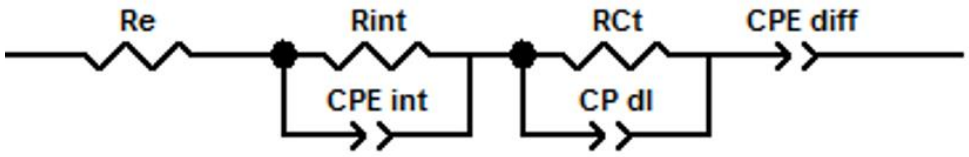

Figure 2: Equivalent Circuit used for EIS

In the context of this thesis, EIS measurements will be used to elucidate the mass transfer differences between the large and small particle electrodes. Figure 2 depicts the equivalent circuit that will be used.

2.8 Galvanostatic discharge

Batteries were evaluated with a coin cell (Cr2035 type). This technique entails a constant current discharge of the battery cells, followed by a constant current charge. The number of electrons transferred are counted from the start to the end of the cycle. The cycle ends when the voltage reaches a specific target voltage set by the user. In the case of LIS, typically fresh cells are first charged to 2.8 V vs Li/Li^+ followed by discharge to 1.9 V vs Li/Li^+ with a ten minute rest between charge and discharge. The current of discharge/charge is called the C-rate and is defined by the following equation:

$$C_{rate} = \frac{1}{Time\ of\ Discharge}$$

Equation 5: C-rate equation

Time of discharge is in hours. One important note to point out is that the discharge time can be based on a many different factors in the battery. Therefore, the discharge time can vary greatly between research papers. As a matter of fact the goal of many studies is to maximize the time of discharge which is an artifact of achieving high specific capacity, the main goal in LIS papers. Due to this variation, the convention used in most LIS research studies is to base the C-rate on the theoretical discharge time of sulfur. For example, theoretically, one gram of sulfur in a battery would take 1675 mA to discharge in one hour, assuming a completely theoretical (100% efficient) use of sulfur. Therefore 1675 mA would be called 1 C, a 30 minute discharge (1675/2 mA) would be 2C and a 10 hour discharge (1675/10mA) would be 0.1C. Galvanostatic cycling will be used to emulate real operation of the LIS in attempt to evaluate its cycle life performance.

Rate performance evaluation is done by ramping the C rates from an initially low rate (0.1C) to higher rates (5C). This is followed by recovery to the initial slow rate to show reversibility in the rate performance. This test will be used to determine the performance of nitrogen doped porous carbon at different current densities which again emulates real operation. It is expected that the nitrogen doped

porous carbon material will significantly outperformed the regular carbon black sulfur composites in both cycle performance and rate performance.

3.0 Application of nitrogen doped porous carbon for LIS

3.1 Introduction and purpose of study

Of the many different types of methods used to mitigate the negative properties of LIS, nitrogen doped carbon has shown great promise. A relatively new application in LIS, nitrogen doped carbon is able to attract polysulfides (PS) through its effect on the electron density in carbon. Nitrogen doped carbon has three different forms: graphitic, pyridinic, and pyrrolic. Graphitic nitrogen generates a slight dipole because it is more electronegative than carbon. Pyridinic nitrogen has relatively strong basic properties because its lone electron pair is not resonance stabilized like the pyrrolic nitrogen. It is believed that the graphitic form of nitrogen has the least effect on PS adsorption. Conflicting simulation results have been reported as to whether pyrrolic[16] or pyridinic [20, 33]nitrogen is more effective for PS adsorption. Whichever the case, nitrogen doping has clearly improved the capacity, cycle life and rate performance [20, 21, 33, 34].

The purpose of this study is to obtain a baseline to improve upon. The novelty of this part of the project is relatively low but provides evidence for two very important properties of small particle NPC.

1. Nitrogen doped porous carbon can indeed improve capacity over typical carbon black/sulfur cathodes.
2. Small particles are inadequate for high loading due to its poor capacity and electrode manufacturability.

3.2 Experimental methods

Synthesis of Nitrogen Doped Porous Carbon:

The procedure implemented are similar in nature to the following publication [35]. A schematic in Figure 3 depicts the procedure.

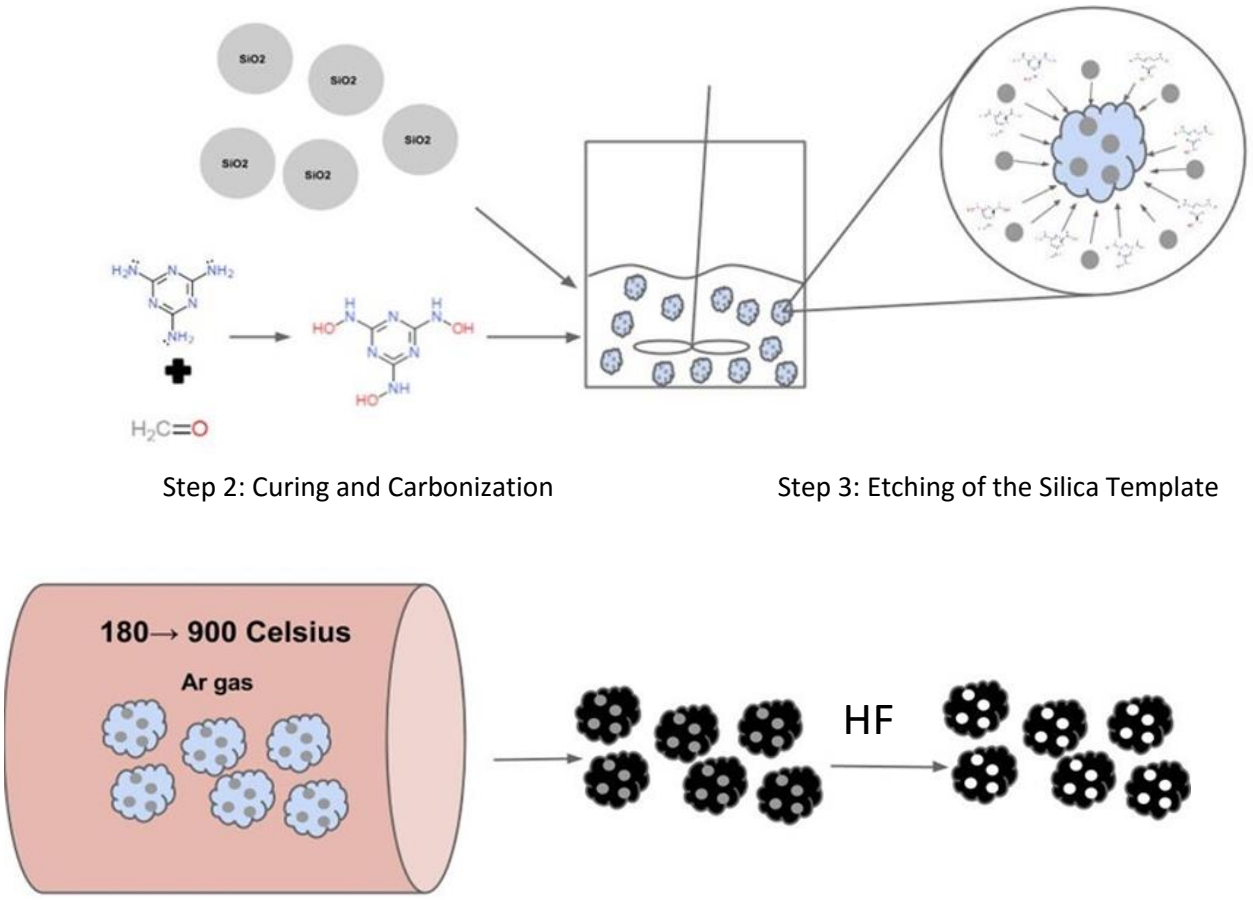

Figure 3: Schematic of the synthesis of nitrogen doped porous carbon

In a typical synthesis procedure of N-doped melamine formaldehyde porous carbon (NPC) 25 ml of distilled water is added to 6.3 g of melamine and 10g of a 37% formaldehyde solution. This is followed

by addition of 2M sodium carbonate until a pH of 8.5 is reached. The obtained mixture is heated to 80 °C under vigorous stirring (750 RPM) until the solution becomes clear. The basic conditions increase the nucleophilicity of the amine group on the melamine, facilitating its attack on the formaldehyde. This forms a water soluble prepolymer solution of methylol melamine, as shown in Figure 4 [36].

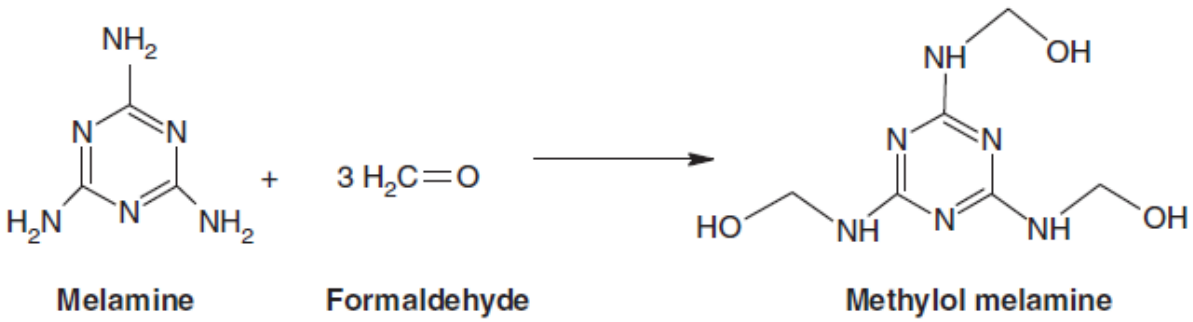

Figure 4: Chemical structure of reactants of products of prepolymer formation[36]

The solution was stirred for 15 minute and then cooled down at room temperature to 40 °C to halt polymerization. A 60 g solution of 5% wt silica suspension (Ludox AS40) was added into the mixture and stirred at 40 °C for 20 minute to ensure intimate mixing. 2M HCl was slowly added into the above mixture until the pH reached 5.5 and stirred for 15 minute. The polymerization of methylol melamine is a condensation reaction that generates water. The acid takes the role of a catalyst leading to the formation of ether linkages between monomers. The stirring was then halted and the solution above was allowed to polymerize in stagnant conditions for 4 hours. After 4 hours, a visible separation appeared between precipitated polymerized melamine formaldehyde resin (MF) on the bottom and the bulk water phase in the top section. The top water phase was decanted, and the remaining white-slurry like material was dried in a 60 °C vacuum oven for 48 hours to remove remaining water. After drying in a vacuum oven at 60 °C , the sample was heat-treated at 180 °C for 24 hours to dry and obtain a near 100% conversion of the condensation polymerization reaction between melamine formaldehyde molecules. The sample was then carbonized by ramping from 25°C to 900 °C at 5°C min^{-1} under argon atmosphere. The silica template was subsequently removed by carefully dispersing in 10% hydrofluoric acid solution for 24 hours. The

remaining porous carbon solid was further carefully washed with distilled water to remove all of the residual hydrofluoric acid (HF).

Synthesis of nitrogen doped porous carbon/sulfur composite:

All NPC and S composites (NPC/S) were synthesized by the typical melt diffusion method, where the appropriate amount of S and NPC was mechanically mixed well in a mortar. The mixture was placed in an argon filled Teflon lined autoclave and heated up slowly to 155 °C and held at that temperature for 12 hours [18]. The sample with 70% sulfur loading is referred to as NPC/70. The Ketjen black (600 JD) and sulfur composite were also synthesized in the same manner as NPC/70.

Electrode Fabrication:

For the smaller particle electrodes, a water based slurry of 15% solid content was formed with the mass ratios of NPC/S: carbon nanotubes: sodium carboxymethyl cellulose as 80:5:15, respectively. The slurry was casted onto a carbon-coated aluminum foil current collector (purchased from MTI) with a typical loading of $1mg_{Sulfur}$ cm^{-2}. The thicker electrode slurry contained 25% solids and 15 % binder; the remaining material was NPC/S and carbon nanotube at a ratio of 80 to 5. All electrodes were dried at 55 °C for 24 hours before being transferred into an argon filled glovebox (Labstar MB10 compact, mBraun) with water and oxygen levels both under 1 ppm.

Electrochemical tests:

The electrochemical performances were evaluated using a 2035 type coin cell with a 1,3-dioxolane and dimethoxyethane electrolyte at a 1:1 ratio with 1M LiTFSI with 0.2M lithium nitrate (pre-blended by BASF). Electrochemical testing station from Neware was used to perform all electrochemical tests. The counter electrode used was a lithium metal chip (Linyi Gelon LIB Co., Ltd) while Celgard 2500 was used as the separator. The coin cells were cycled from 2.8V to 1.6V vs Li/Li+ for the rate performance test. All other cycles were performed from 2.8V to 1.9 V vs Li/Li+ to avoid irreversible decomposition of $LiNO_3$ on the cathode [37] at the cost of some capacity loss.

3.3 Results and discussion

Confirmation of material morphology and doping:

Before a high loading electrode is to be fabricated, we must establish a baseline and find a suitable material that has exceptional performance as a small particle. Conductive additives are required to deliver electrons to the sulfur. When sulfur infiltrated into the pores of porous carbon, the electrons can conduct through the walls of the porous carbon to reach the sulfur. Nitrogen doped porous carbon (NPC) derived from melamine was selected due to the widely available literature on its synthesis [35]. NPC was synthesized *via* a silica-templated *in situ* polymerization of melamine-formaldehyde resin (MF). The procedure implemented was very similar in nature to the following publication [35]. The resulting NPC material was studied using scanning electron microscopy (SEM) as shown in Figure 5 (a) and could be described as a mesoporous carbon particle of around ~500 nm. The material is not of a perfectly shaped sphere most likely due to the lack of mixing and absence of surfactant-like chemicals during polymerization.

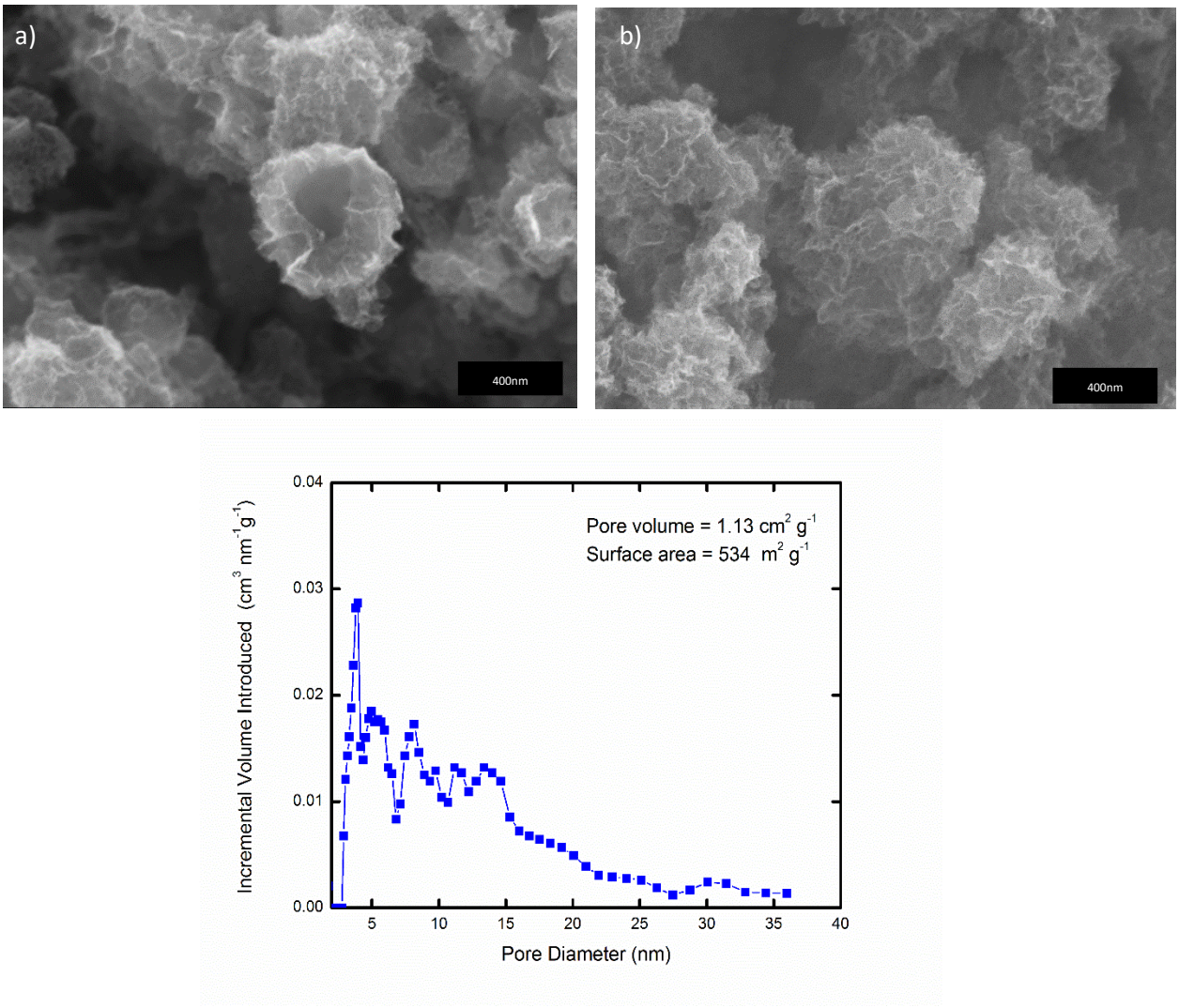

Figure 5: NPC with Silica Removed with 0% wt sulfur (a), SEM of NPC with 70% wt sulfur (b) and Pore Size Distribution (c)

BET analysis revealed that the material has a surface area of 534 $m^2 g^{-1}$ and pore volume of 1.66 $cm^3 g^{-1}$. Furthermore, the pore size distribution of NPC showed that it not only possessed 10-20 nm mesopores but also micropores. As a matter of fact, the amount of micropores (2.5 nm to 10 nm) represent a much larger portion of the pore volume than the mesopores. This occurred most likely due to the volatiles generated upon carbonization leaving behind empty space, i.e. pores. The combination of a high surface area and pore volume ensured a high uptake of all S into its pores and not on the surface. Sulfur was melted and

heated to 155°C. The melting point of sulfur is 115°C, 155°C was selected because the viscosity of sulfur is at its minimal versus temperature. Above 155°C the sulfur will start to polymerize and crosslink with itself resulting in an increase in viscosity to about a maximum of 178°C. Upon reaching 155 °C, sulfur is sucked into the pores of the carbon through capillary action, also known as the melt diffusion method [10] and impregnates the carbon. If the pore volume and surface area of the carbon are sufficiently high, all the sulfur will be accommodated into the pores of the carbon and will be not be found on the surface of the carbon.

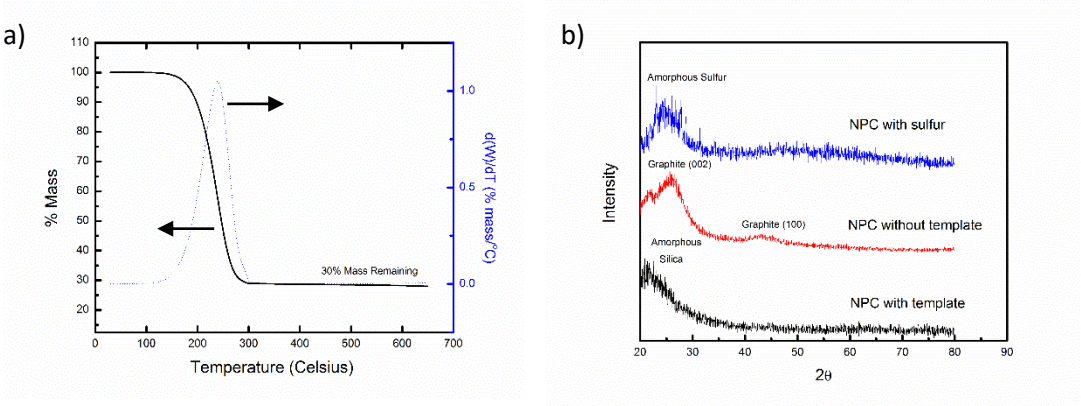

Figure 6: TGA curve of NPC/sulfur composite (a) and (b) XRD pattern during various steps of NPC synthesis

TGA results shown in Figure 6 (b) confirms the S percentage in the composite is ~70% wt in the NPC/ S. After heating to 650°C in nitrogen atmosphere the mass reduced to 30% indicating a 70% mass loss or more specifically, sulfur mass loss. It should be noted that although the boiling point of sulfur is 444°C the first derivative of weight with respect to temperature peaked at ~250°C . This is consistent with literature and is most likely due to absence of sulfur in the inlet nitrogen gas creating a sufficiently large sulfur concentration/vapour pressure gradient facilitating the evaporation of sulfur. Moreover, no generation of CS_2 through the oxidation of carbon by sulfur will occur as the temperature is kept below 850 °C. This is crucial to ensure an accurate estimate and avoid convolution in the weight vs temperature curve. Avoidance of carbon oxidation was further confirmed by the lack of peak in the first derivative of

the weight with respect to temperature. The X-ray diffraction (XRD) pattern (Figure 6 (b)) of the composite prior to hydrofluoric acid treatment indicates the presences of silicon dioxide. As expected the silicon dioxide peak disappears after hydrofluoric acid treatment (NPC without template), leaving behind a peak indicating the existence of a slight graphitic carbon material. Finally, after S infiltration, the composite XRD pattern reveals that no sharp S peaks can be found. This indicates the existence of a thin near amorphous or very fine crystallites of S film [38] both of which are beneficial to performance. This is further corroborated by SEM images (Figure 5 (b)) of the composite showing no apparent large S agglomerates or even the presence of sulfur. The thin S film is a very important advantage of NPC for LIS. Derived from its pore volume the ability of NPC to efficiently accommodate and distribute S evenly prevents possible agglomeration of S. Therefore, a large portion of the loaded S is thin enough to be electronically active. It should be noted that although the initial activation of S is important, theoretically it should only contribute to ~33% of the overall capacity and merely represents the initial conversion of S into the electrolyte-soluble higher order polysulfide species (8th to 6th order). The remaining capacity lies in the ability of the electrode to retain and discharge/reduce the dissolved higher order PS into the lower order lithium sulfide (4th to 1st)[7, 8]. Because the intermediate polysulfide species are all soluble in the electrolyte, the cells functions not as a regular battery cell but as a catholyte cell with corresponding mass transfer complications. The reactant is constantly being stripped from the electrolyte and the soluble product is generated in the electrolyte. As expected the reduction of these PS species directly competes with the diffusion of the same PS species away from the reduction sites. Any diffusion away from cathode can lead to unwanted side reactions, either precipitation onto the nonconductive parts of the cell [7] or a direct short circuit on the lithium anode. Fortunately, the increase in complexity and distance of the diffusion length stemming from the micro/mesoporosity of NPC significantly hinders mass transfer of the PS out of the cathode. Furthermore, the nitrogen doped sites present in NPC also can acts as PS adsorption sites retaining PS close to nearby reduction sites [20, 21, 33, 39]. The nitrogen-rich melamine provided the opportunity of creating porous carbon with nitrogen doping. X-ray photoelectron spectroscopy (XPS) was performed to confirm the presence of nitrogen in the synthesized porous carbon.

Figure 7 displays the XPS spectrum, indicating nitrogen doping at binding energies levels of 400.8 eV, 399.3 eV and 398.1 eV, stemming from the graphitic, pyrrolic and pyridinic forms of nitrogen, respectively [40-43]. In total the nitrogen content in NPC is ~15%.

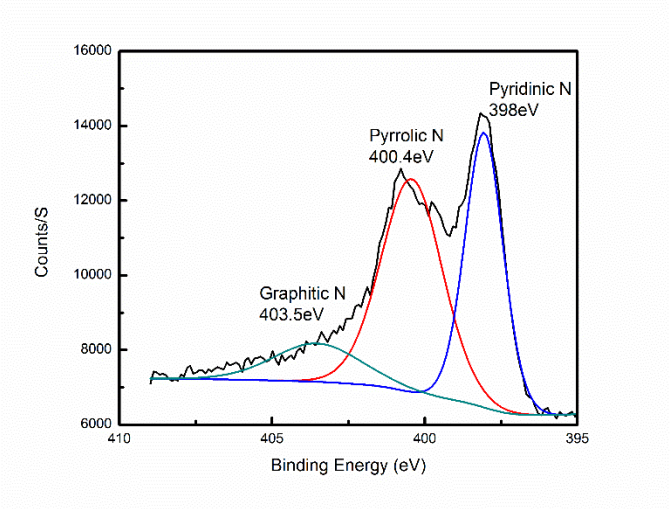

Figure 7: XPS spectrum of NPC

Described in literature, nitrogen doped carbon material has displayed great promise in LIS application. Based on experimental methods [20, 34, 39, 44] or theoretical simulations [20, 21, 45], nitrogen-doped carbon has been shown to have an affinity for PS. More specifically, its ability to attract and adsorb the PS on the surface of the NPC hinders PS diffusion out of the pore structure makes it a good possible candidate. There are three forms of nitrogen-doping, pyrollic, pyridinic and graphitic. The working principle of all forms of nitrogen-doping is similar, electrostatic interaction of some form is introduced allowing for the attraction and adsorption of lithium polysulfide onto the surface of the doping site. Graphitic nitrogen is the weakest form because its electrostatic interaction is only a function of the dipole generated from a slight difference in electronegativity between the carbon and nitrogen. Therefore, it is desirable to decrease the amount of graphitic nitrogen in the carbon. In our case the amount of graphitic nitrogen was only atomically 12.5%. Although, it should be noted that no formal optimization was performed to obtain this low graphitic nitrogen content. We believe this low graphitic content is owed to

the short carbonization time of 2 hours. Graphitic nitrogen is the most stable of all the nitrogen doping as it is intimately incorporated into the carbon graphene structure. If the carbonization was allowed to proceed past 2 hours the pyridinic and pyrollic forms could decompose and raise the graphitic nitrogen percentage. Often time, the pyridinic form of nitrogen doping is referred to the most effective for PS trapping because of it lone pair electron. While the pyrollic nitrogen does also have an electron pair, the lone pair on the pyridinic is not resonance stabilized. Because the lone pair on the pyrollic nitrogen is resonance stabilized it is inherently less basic than that of its non resonance stabilized counterpart, the pyridinic. In our NPC material, the pyridinic form atomically represented 48.5% of the nitrogen while the pyrollic form represented 39%. Again, no formal optimization was made to obtain this, but it should be noted our NPC material does have a high amount of nitrogen doping that is particularly beneficial to PS adsorption, i.e. pyridinic and pyrollic. Adding to electrically active sites and PS diffusion, nitrogen doping is now qualified as another competitor for PS mass transfer. We believe the excellent cycle stability Figure 8 (a) attributes to the ability of nitrogen-doped carbon to limit the PS diffusion and restricts PS migration out of the cathode.

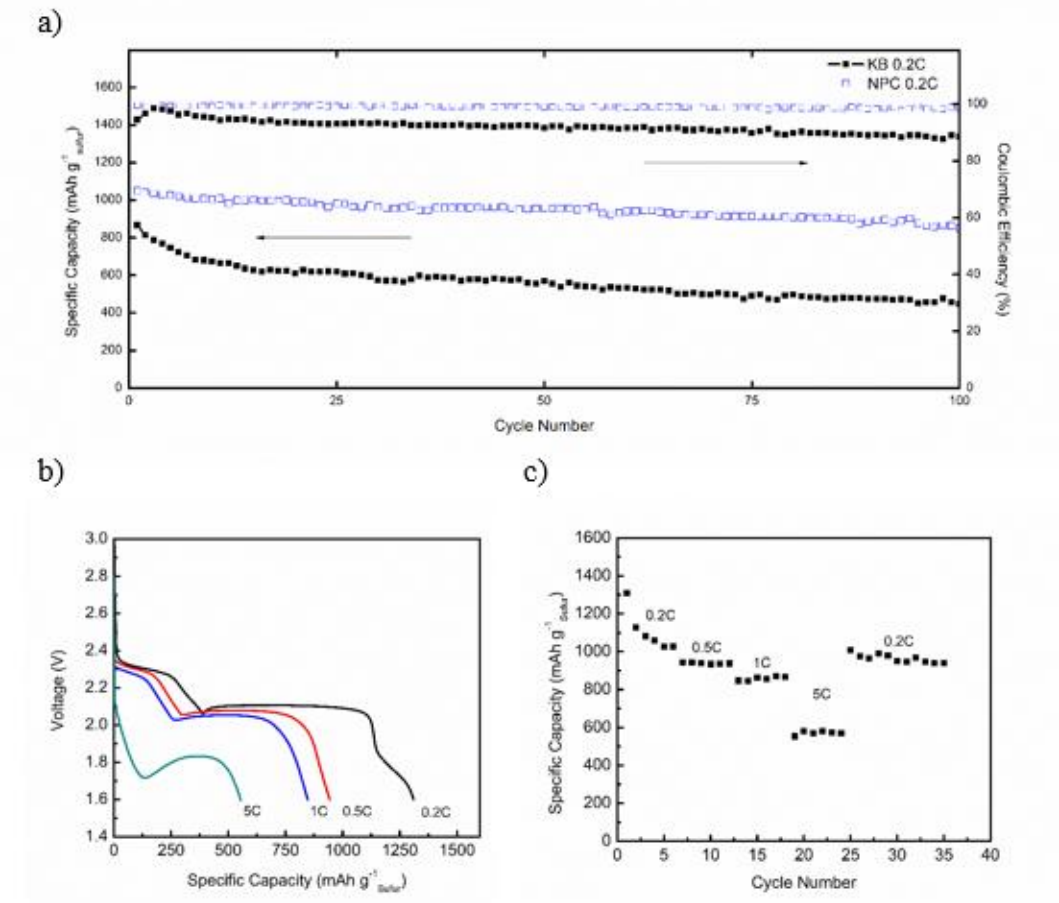

Figure 8: Electrochemical data, a) cycle life evaluation of NPC and Ketjenblack 600 JD (KB), b) voltage curves of rate performance, and c) rate performance

The ability of NPC to hinder PS diffusion was again shown in cycling stability data (Figure 8 (a)) with a capacity retention of 81% after 100 cycles at 0.2C. To contrast, a drop of capacity of KB from ~870 mAh g^{-1} to ~450 mAh g^{-1} in 100 cycle (51% retention) is observed. Cycle stability of the cathode depends on the ability of material to repeatedly deliver electrons to the same amount of the previously deposited S on discharge and re-deposit that same amount S during charge. Moreover, the coulombic efficiency (defined as the percentage of the charge cycle that is achieved in the subsequent discharge cycle) decreased much quicker than that of NPC. As described previously, the shuttle effect/diffusion of PS to the anode works directly against the act of charging. Therefore, because the KB electrode is not able to retain the PS inside

the electrode structure, the PS escapes and short circuits at the anode. As a result, more energy is required to charge the KB LIS than what can be taken out i.e. a poor coulombic efficiency. It is imperative to not provide too much free diffusion pathway and prevent quick PS diffusion from the cathode resulting in permanent capacity loss. Based on the impressive cycle stability of our NPC it was reasoned that NPC offers sufficient mass transfer hindrance to keep the dissolved PS during discharge at close enough proximity to achieve a near 100% re-deposit of all soluble PS into insoluble lithium sulfide at the end of discharge. On the other hand, KB was not able to retain PS as it only relies on the interparticle pores to decrease the effective diffusion coefficient and does not have the benefit of nitrogen doping.

While NPC offers significantly improves S utilization and cycle stability, another impressive aspect of the NPC material is its exceptional rate performance, as seen in Figure 8 c), NPC is able to discharge up to 5C delivering a capacity of around ~600 mAh g_{sulfur}^{-1}. Although the C-rate performance depends on many different factors, we believe that this occurs mainly as a results of the combining effects of nitrogen doping, the geometrical stacking of the ~500 nm NPC, and the micro and mesoporous pores of the material. Nitrogen doping which has been shown to have a catalytic effect on the S reduction reaction by decreasing the onset potential for the reduction [46], reducing charge transfer resistance and could

partially explain the excellent rate performance observed in NPC. Furthermore, the rate of lithium ion diffusion has to be sufficiently high to support reaction rates up to 5C.

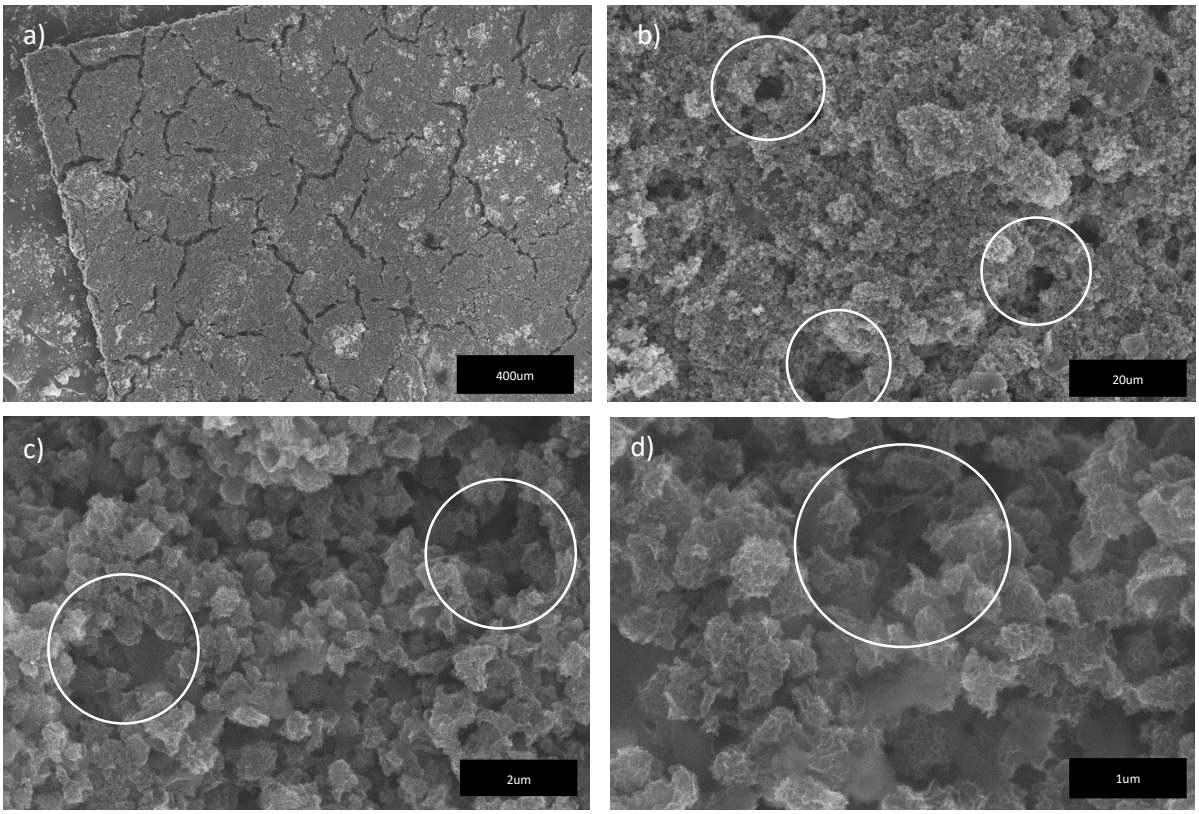

Figure 9: Electrode of NPC, 50X (a), 1000X (b), 10 000 X (c) and 50 000 X (d) with macropores indicated by white circle

This was made possible through the use of a hierarchical electrode. A hierarchical electrode architecture contains large macropores and smaller mesopores exist. In the case of the NPC electrode, the walls of the macropores are made up of NPC particle particles which possessed mesopores. The existence of such an architecture is due to the ability of the NPCs to stack upon one another with sufficient void space due to the relatively large particle size of NPC (~500 nm). Visually speaking, in Figure 9 c), the small particles forms interparticle pores and interparticle-cluster pores of various sizes. Micropores and mesopores restrict PS diffusion out of the cathode (Figure 9 d)) but it is the macropores that plays the crucial role in efficiently delivering lithium ions to the S at high current densities [47]. It creates an efficient lithium ion mass transfer highway that could endure rates up to 5C. Another contributing factor for the observed rate

performance is the previously mentioned high surface area of the carbon material allowing for uniform deposition of lithium S and subsequent re-deposition of S throughout cycling. The increase in contact area between the carbon scaffold and S has two main advantages, the decrease in the size of electronic insulator (thickness of the S coating) due lower S loading per surface area and the local current density which both contributes to a lower absolute value of ohmic losses. This ultimately allows for access to a large amount of S even at high C-rates. NPC was able to deliver improved performance as a sulfur host for LIS.

Moving towards an increase in the areal loading of sulfur/ specific energy density of electrodes, a thicker slurry film needs to be fabricated. Unfortunately, with the small particles, we quickly found it nearly impossible to fabricate a uniform electrode of thickness (dry) anywhere greater than 30um. Figure 10 illustrates the visibly cracked electrode surface and the pin holes (circled in white) even at high binder content (15%).

Figure 10: Digital photograph of attempted 4mg cm^{-2} loading small particle NPC electrode with 15% binder, pinhole indicated with white circle

A decrease in particle size creates smaller interparticle pores in which the slurry solvent resides, amplifying the effects of capillary action during evaporation. The binder acts as a bridge between particles to dissipate stress generated during drying through its elastic nature. If no binder exists between dispersed particles in slurry, the particles would succumb to capillary action during the drying process, aggregating and generates a large stress throughout the surface of the electrode. If the stress is sufficiently high, the electrode would either crack, curl, form pin holes or delaminate [23, 29], all of which is debilitating for quality assurance during manufacturing. Also if the particle size is small, a large demand for binder would exist due to the increase in surface area to be glued together. Consequently, from our experiments, the small particles required 15 wt% of binder to even obtain a mere 1 mg cm^{-2} loading and upon reaching 4 mg cm^{-2} cracks were evident. Therefore, to obtain a practically high loading we would

require an even higher increase binder. Unfortunately this is not practically feasible since greater than 15% binder is not commonly reported even in literature [32, 48, 49]. Not only does a higher binder content pose a possible economic concern it could also compromise the crucial conductive network throughout the electrode. Finally, the most detrimental drawback of a higher binder content is a decrease in active electrode material and consequently decreases the specific energy density which nullifies the benefits of using sulfur in the first place. By using larger NPC particle, the amount of required binder would decrease because the outer surface area would decrease. Less binder would be needed to adhere all the large particle together. Large particle would also produce larger interparticle pores and would reduce the capillary action of the evaporating water during drying.

Even if a thick electrode was obtainable for the small particle, the large increase in binder content (>15%) decreases porosity and would drive up the overall Thiele modulus of the electrode to the point where most of the sulfur cannot be reach by the lithium ions. To add to this, the mere act of increasing the thickness of the electrode would also increase the Thiele modulus of the electrode. The small particles naturally possess smaller interparticle pores, although the small particle can form micron sized clusters with larger inter-cluster pores seen in Figure 9 (b-d), there would not be consistently enough of it throughout the electrode. This is the key point in the next part of this thesis. If the random aggregation of the small particle NPC was to be controlled, then every single small particle could be part of a micron sized cluster. The increase in average effective particle diameter or clusters would increase the average interparticle pore size throughout the electrode and finally the porosity of the electrode would increase. Motivated by these two points: ease of electrode fabrication and promotion of lithium ion mass transfer, a method to increase particle size was sought.

3.4 Section Conclusions and remarks

A nitrogen doped porous carbon synthesized by silica hard templated pyrolysis of melamine formaldehyde resin. After fabrication of electrode of 1 mg cm^{-2} we compared NPC with KB and found that NPC had a more stable cycle life, higher capacity. Furthermore NPC also possessed excellent rate performance. From attempts to fabricate a high loading electrode (4 mg cm^{-2}) it was quickly realized the electrode quality significantly deteriorated. This destroys any possibility of using electrode on a large scale production line. After some literature search it was found this related to the particle size of the porous carbon, hence a method for increasing particle size became the topic of the next set of experiments.

4.0 Development of large diameter porous carbon for high loading LIS

4.1 Introduction

From the last study it was hypothesized and supported by literature [23, 24] that there are problems associated with small particles in higher loading electrodes. In this study, the large particle's potential benefits of lower binder requirement, larger interparticle pores are presented. To increase the particle size of NPC one must understand the mechanism of its synthesis. The method used in our procedure is still a type of dispersion polymerization but in the presences of a chemically inert hard template. Hence it is to be expected that seed crystals form or in this case the birth of seed particles mixed with template (seed composites). This is followed by the aggregation of the seed composite. The third step is the subsequent growth of these aggregates [50-52]. The typical procedure to increase the particle size of MF is to raise the concentration of MF pre-polymer [50-53]. Indeed this is quite a simple and facile method, but to increase concentration of a resin's pre-polymer solution could result in a very serious risk of uncontrolled crosslinking during manufacturing. Therefore we decided to pursue a much more direct method for controlling particle size. Through modification of the surface charge and the resulting spike in rate of seed aggregation with NaCl, we have successfully increased the particle size. NaCl was strategically chosen to be added early on in the synthesis process, we believe addition at 16 minute is during the seeding stage of the reaction. This theory is supported Wu et al 's investigation into the pure MF particle formation as a function of time [50] shown in Figure 11.

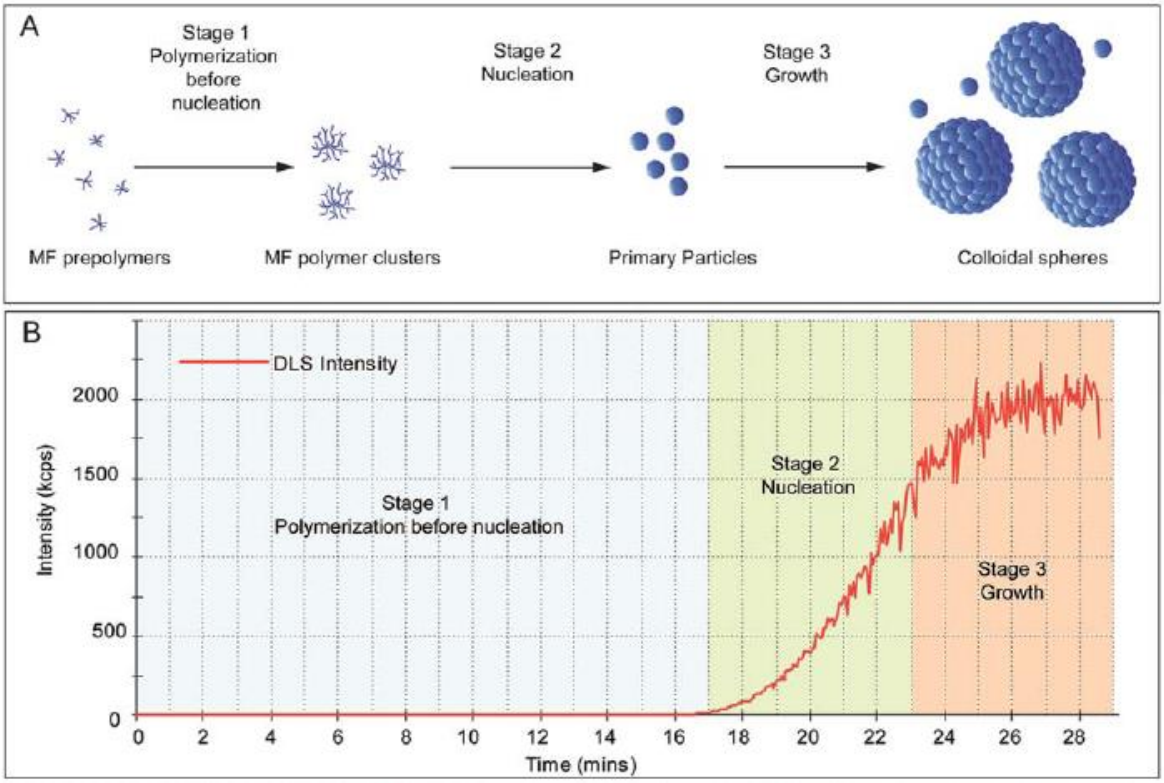

Figure 11: Mechanism of growth of colloidal MF spheres [50]

4.2 Experimental methods

Synthesis of large diameter nitrogen doped porous carbon:

Synthesis of the larger particle (LNPC) was identical to the procedure in the previous section (small particle) except that 5% NaCl was added 10 minutes after HCl addition and stirred for another 5 minutes adding up to a total of 15 minute of total stirring after acid addition. The weight percentage of NaCl is relative to the water content in the system.

Synthesis of freestanding Ketjen black electrode

18.5g of Ketjen black (KB)/sulfur composite was sonicated in solution of 7.5ml of water and 7.5ml of ethanol for 15 minute. To follow, a 1.5g of a 5% by weight PTFE suspension was added dropwise to the above slurry and sonicated for another 15 minute. The slurry was stirred at 300 RPM for 30 minute and subsequently dried at 60 ^{o}C for 12 hours. After being dried, 3ml of ethanol was added to the dried slurry upon. The resulting slurry was a very malleable bread-dough like paste. This paste was rolled pressed to a certain thickness (100um) to obtain the desired loading (4mg cm^{-2}).

All other experiments were performed similar to the first study.

4.3 Results and discussion

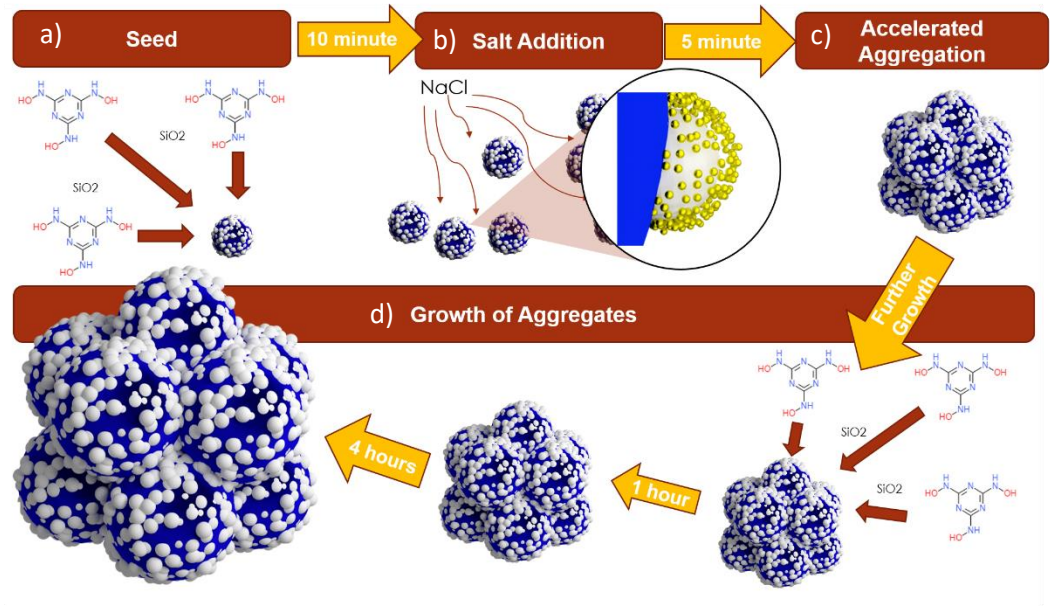

Figure 12: Schematic of particle growth mechanism (blue = melamine formaldehyde, white = silica template and gold = sodium ions)

Figure 12 displays a schematic of the mechanism of how exactly the particle size increases. The main difference between this schematic and Figure 11 is the presence of the silica template. The mechanism proposed here is a direct analog of that of pure MF polymerization. Initially, MF would polymerize onto the silica which would aggregate with other MF wrapped silica templates to form MF/silica composite seeds (Figure 12 a)). After addition of NaCl these small aggregates are further combined forming larger particle clusters as shown in Figure 12 b)-c). MF will then further grow from the surface of these particle outwards increasing size during the zero RPM (stagnant) phase of the synthesis (Figure 12 d)). The resulting product (shown in Figure 13) displays a large particle of 2.5um across composed of smaller particles indicated by yellow circle. The small particle is about 500nm in alignment with SEM images of small NPC particle described in the previous section.

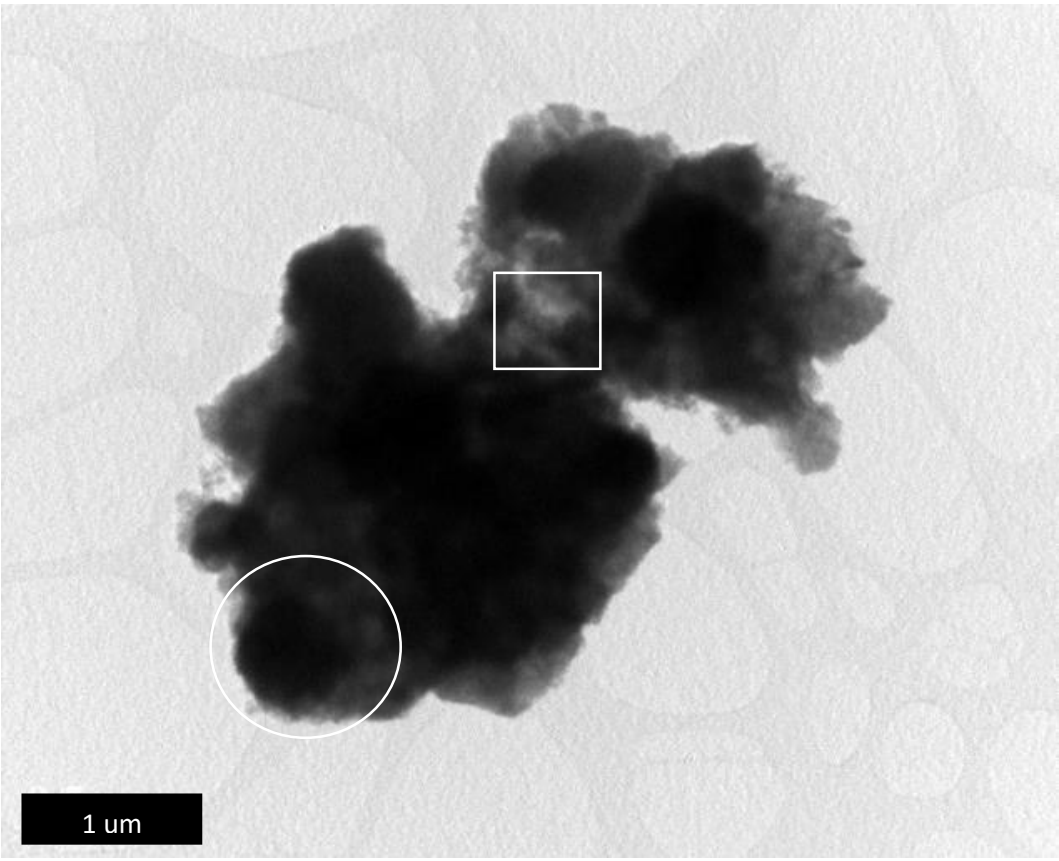

Figure 13: TEM image of MF/silica aggregates, white circle indicate the smaller particle NPC, white box indicates the extra MF "glue"

The mechanism of which this large particle was synthesized was supported by zeta potential measurement. The synthesized composite material without NaCl (small particle) had a surface charge of around -9.95 mV. Positive sodium ions adsorbed onto the surface of the negatively charged surface of the seed particles and lowered the surface charge to -1.67mV (Figure 13 (a)). Notice that the zeta potential was not particularly high to begin with (-9.95 mV), implying that these particle would eventually aggregate over time. This means that adding NaCl does not in a sense induce aggregation, but instead, amplifies/accelerates the aggregation during the second stage of the particle synthesis process. We propose that through this technique, larger aggregates were produced early on in the synthesis process. This specific polymerization could be classified as a precipitation polymerization, which at some point must seed, aggregate and precipitate. From visual inspection (not shown), the solution started to cloud up even without NaCl addition after about 30 minutes of stagnant polymerization. When NaCl is present, the

time of reaching a significant turbidity shortens so that it occurs immediately after the salt addition. This indicates that NaCl affects the aggregation speed. With an increased size of seed composite aggregates, we have shifted the baseline size from which the particle will be further grown. Moreover the TEM image (Figure 13) reveals that the large particle is not only an aggregate of small NPC but that polymerization occurs between the smaller particles (lighter regions). This implies that after aggregation, further MF polymerization "glues" the small NPCs together. This is important to prevent breakage of the large particle during subsequent processing to the synthesize sulfur/NPC composite and formulation of the slurry.

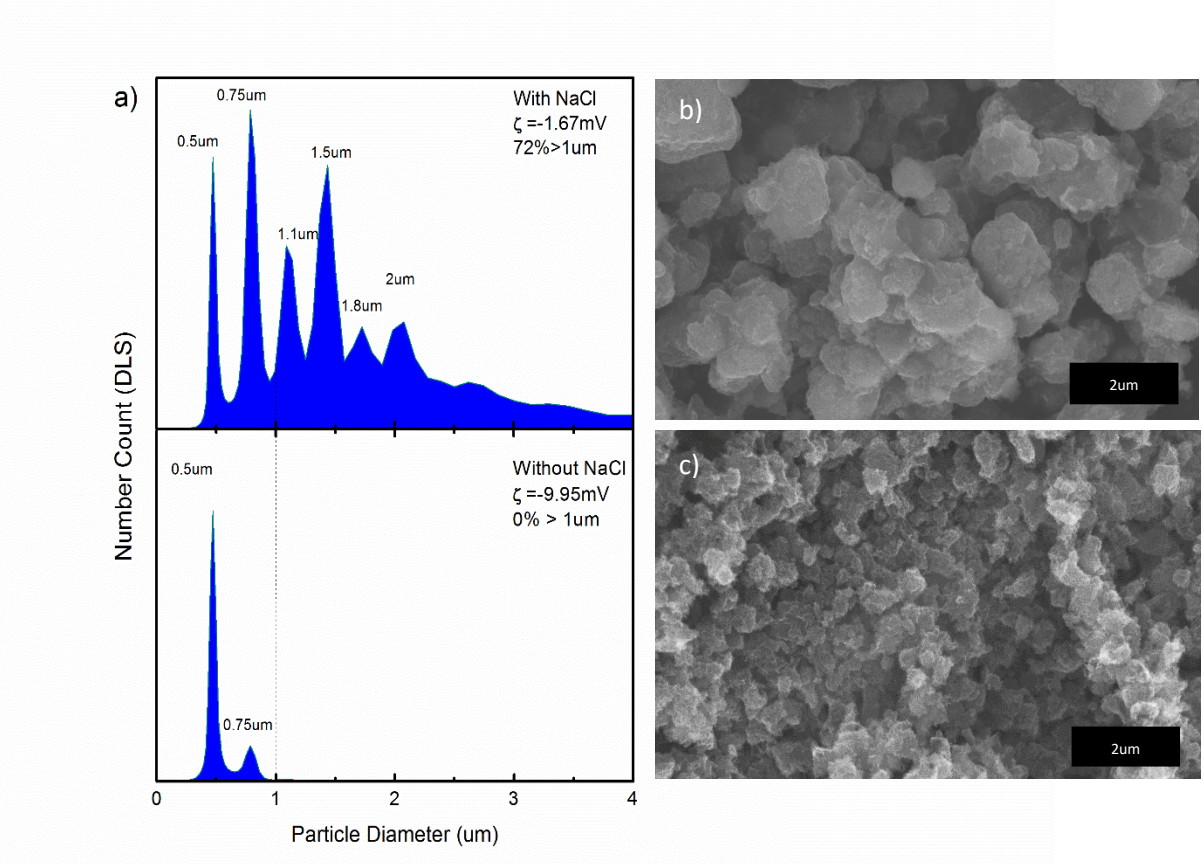

Figure 14: 5% salt DLS particle size distribution (a), 5% salt SEM image (b), No salt DLS particle size distribution (c) and No salt SEM image (d)

To confirm the particle size increase, SEM and dynamic light scattering (DLS) were used. As shown in Figure 14 a), the addition of NaCl has a drastic effect on the particle size distribution. Just by visually inspecting the sample under SEM, the particles increased in size from 500 nm to 1-2um (Figure

14 (b)). For a more rigorous quantification, DLS measurements were performed. The sample without any NaCl displayed a relatively sharp distribution at around 500 nm in agreement with SEM images. A peak at around 750 nm also appeared suggesting that some agglomeration due to Na^+ present from the use of Na_2CO_3 in the early stage of prepolymer preparation. After NaCl addition the distribution shifted to the micron scale with 72% of the distribution above 1 um. The addition of NaCl induced the formation of larger agglomerates of seeds particles which were able to be grown up to the 2um range. Interestingly, the sample with NaCl also had a similar lower bound for particle size. These relatively smaller particles most likely did not get a chance to agglomerate. As part of the coagulation and flocculation technique incorporated in waste water facilities, change of the surface charge is usually used in combination with rigorous stirring to increase rate of agglomeration [54]. It is important to remember that in our case, the mechanical stirring of the beaker was stopped shortly after NaCl addition (20 minute) to prevent non-uniform coating of pure MF on composite surface, shown in Figure 15. This is most likely the result of the change in the mass transfer from stirring to stagnant condition. In the diffusion limited case the monomers would build/polymerize onto the MF polymer chains scattered in a fractal pattern pver all the silica template. This would facilitate better mixing between MF and silica in the final composite as the new monomers would add around the silica. With agitation, it is possible that the MF polymer clusters quickly combined with other clusters not allowing intimate mixing with silica. Furthermore, the agitation can also generate enough shear to break the silica and MF composite. This nullifies the advantage of using a template and hence justifies the choice to operate the polymerization under stagnant conditions.

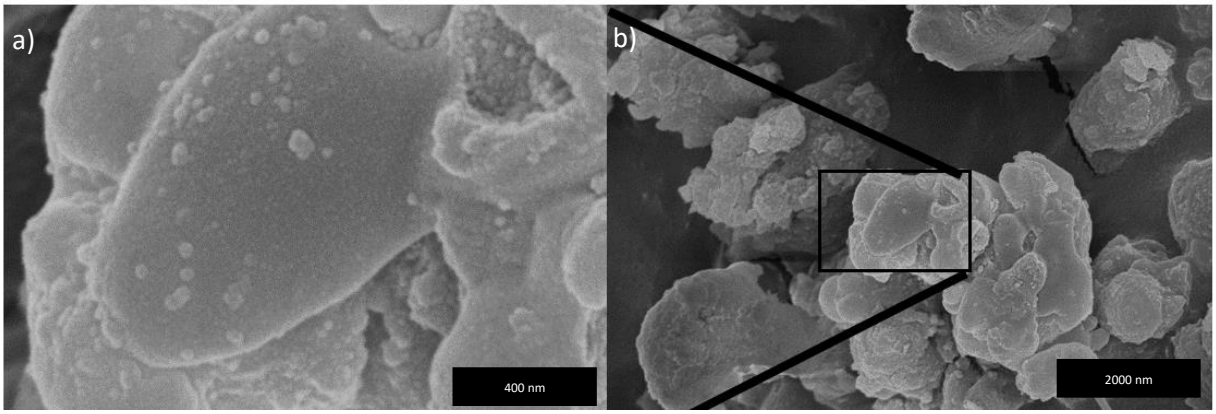

Figure 15: Effect of Stirring on Composite Morphology, a) 50 K magnification onto covered particle b) 10K magnification on covered particle

Coming back to the explanation of the 500 um peak in the large particle, it is also possible that due to mass transfer limitation some of the non-agglomerated MF/silica seed composites did not have a chance to combine with each other. Even if the surface charge was lowered, each particle would still have to be in close vicinity to agglomerate. This led to the formation of relatively smaller seed aggregates that were only able to grow to 500 nm. Ultimately, this formed a cascading multi-modal particle size distribution as an effect of adding NaCl into the synthesis. Nevertheless, the overall particle size distribution shifted to a larger average

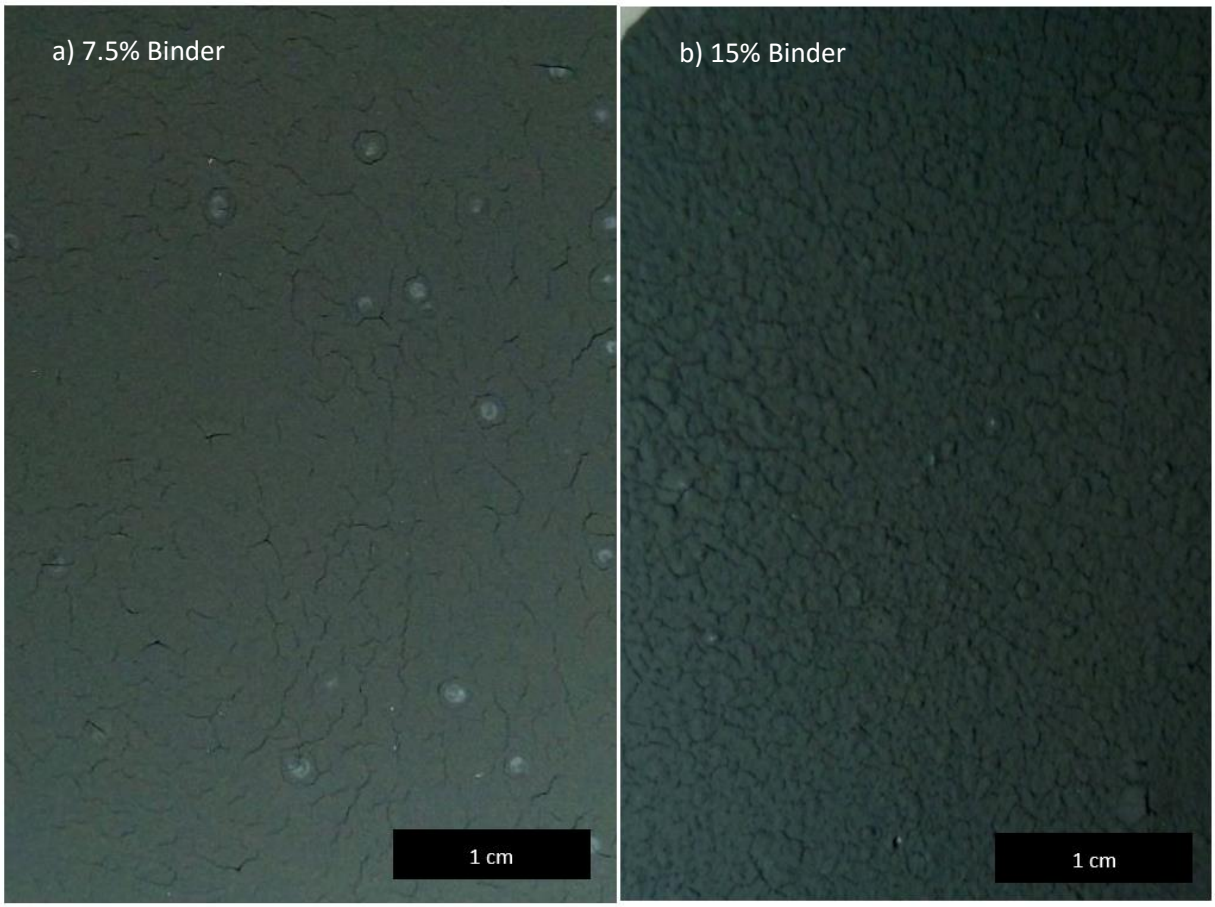

Figure 16: Electrode comparison between large (a) and small (b) particle at ~100um (dry) or ~4mg cm^{-2}

Electrode fabricated from the large particle revealed much improved quality. Cracking of the big particle electrode (Figure 16 a)) is significantly less than that of the small particle (Figure 16 b)). Remember, the binder content was also decreased from the small particle (15%wt) by half to 7.5%wt for the large particle further demonstrating the effectiveness of the large particle in fabricating a robust electrode. It is also important to note that white circular spots/patches appeared in the big particle electrode Figure 16 (b), presumably patches of non-distributed binder. If the binder migrated to these white patches, slightly lower than 7.5% wt binder is present throughout the electrode.

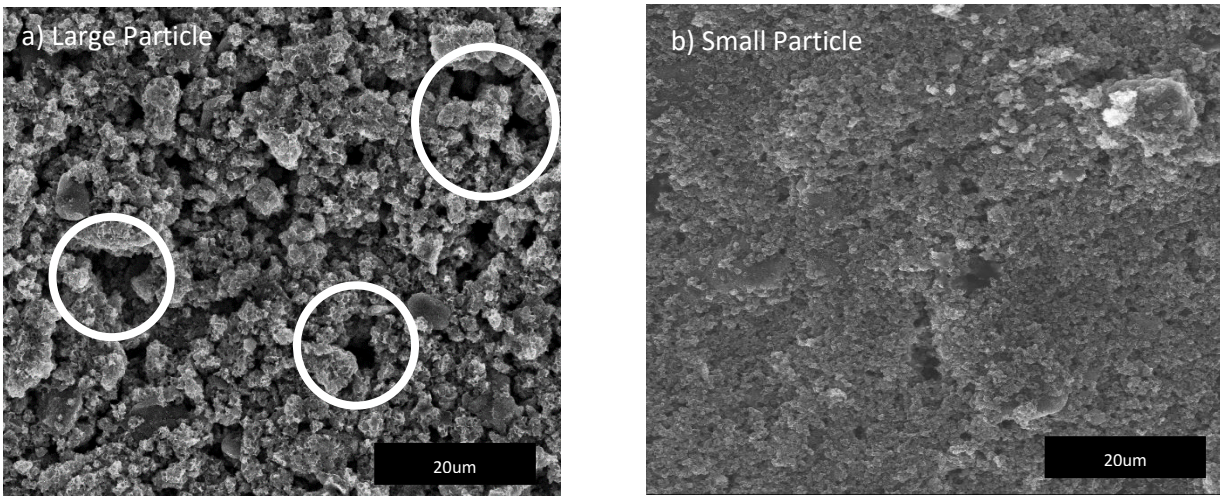

Figure 17: SEM of Large particle electrode at 7.5% binder (a) and SEM of small particle electrode at 15% binder (b)

Furthermore, SEM was used to study the electrode, revealing that the electrode with large particles (Figure 17 a)) was visually very porous (white circles) whereas the electrode with the small particle electrode (Figure 17 b)) was not porous at all. It should be noted that the use of 15% binder in the small particle is more than that of the 7.5% of the large particle. This could result in some convolution in SEM results presented in Figure 17. The porosity in the large particle might simply be due to the lowered binder content. Therefore, equal weight % dispersion of both the large and small particle electrode were drop casted on SEM tape without any binder and dried. Without the use of binder, the SEM images are now de-convoluted and the resulting porosity different was again seen (Appendix B). The large NPC particle still appeared much more porous than that of the small NPC particle. All these results really demonstrates the effect of utilizing large micron sized particles to increase the uniformity of the electrode, in alignment with literature [24].

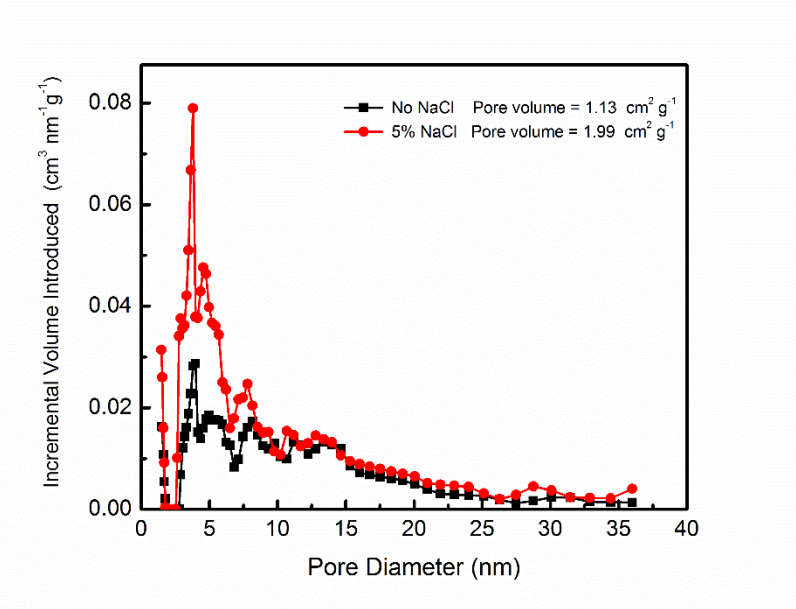

Figure 18: Pore size distribution of large particle NPC

Additionally, another important benefit of adding NaCl was found. The salt can provide a second set of template, forming micropores. The integration of metal ion in the carbon precursor prior to carbonization can lead to pore formations [55-57]. The sodium ions adsorbed onto the polymer surface and support the micropore structure. After carbonization, the surface affinity of polymer (now carbon) for Na^+ most likely changed and during the HF washing procedure the Na^+ was removed leaving behind micropores. From the pore size distribution (Figure 18 a), after NaCl addition, the adsorbed volume of pore sizes up to 7.5 nm increased significantly. These pores are especially useful in acting as PS diffusion barriers. Furthermore the corresponding increase in surface and pore volume will further increase the ability of the porous carbon to accommodate sulfur into its matrix. As mentioned in the last section of this thesis, a higher pore volume and surface indicates that sulfur would be able to homogenously distribute itself throughout the pores of the carbon. This results in a very thin layer of sulfur of which a majority is accessible by electrons.

The large particle was found to form a uniform and robust electrode with only a 7.5% binder. This material was even able to reach loading up to 4 mg_{sulfur} cm^{-2} in agreement with the higher loading publications [20, 21, 48, 58-60]. Any electrochemical comparison with the small particle NPC high

loading electrode could not be done. The medium of testing is a coin cell which requires a circular shape. During the cutting procedure to obtain a small electrode area, the high loading small particle electrode fell apart. The electrode delaminated from the electrode rendering it impossible to test. In order to show the advantage of large particle NPC, a KB /PTFE freestanding electrode was fabricated as a comparison. KB was chosen because it is on the nanometer scale and has roughly a diameter of 40 nm. Therefore, any problem in terms of mass transfer seen in the small NPC particle will no doubt also be seen in the KB with even smaller particle size. Figure 19 (a) shows the difference in impedance between the large NPC and the KB electrode both at 4 mg cm^{-2}. Table 1 compares the fitted parameter values of the commonly proposed circuit [30].

Table 1: EIS fitted circuit parameters

	Large particle NPC	**Ketjen black**
	Resistance (Ohm)	
R_e (electrolyte resistance)	1.858	1.759
R_{int} (interfacial resistance)	13.17	153.2
R_{ct} (charge transfer resistance)	14.87	61.46
	CPE (Siemens sec^n)	
CPE_{diff} (Li^+ conductivity)	1.189	0.0234

Clearly the NPC electrode exhibits lower mass transfer resistance in terms of charge transfer (14.87 Ohms compared to 61.46 Ohms), interfacial (13.16 Ohms compared to 153.2 Ohms) and diffusion (1.189 Siemens sec^n to 0.0234 Siemens sec^n). Charge transfer can be attributed to the nitrogen doping of the NPC while the large difference in CPE_{diff} would most likely be a result of the large interparticle pores due to increase in particle size. This is again seen in the rate performance (Figure 19 (a)) where the NPC material was able to discharge up to 0.5 C with still ~900 mAh g^{-1} while the KB electrode was barely able to reach 500 mAh g^{-1} at 0.2C. The first plateau, attributed mostly to the initial reduction of sulfur to its 6^{th}

order form is interestingly very similar between the two electrodes. While the second plateau which owes to the reduction of soluble polysulfide species is very short in the case of the KB electrode. It is well known in the LIS field that the viscosity is increased when the second plateau is reached since all the sulfur is in the solvated state [30]. In the case of the KB electrode the sudden rise in viscosity was significant enough to increase the lithium ion diffusion resistance. Ultimately this led to the premature drop in voltage past the cut-off voltage of 1.5 V. In the case of the large NPC particle this was not observed. Therefore, both the KB electrode and large NPC particle was able to have high enough surface area to reduce sulfur to high order polysulfides but at the second plateau the large particle NPC was clearly superior. In addition the voltage of the second plateau is lower in the 0.5C compared to the 0.2C which is to be expected as the higher rate would induce a more rapid formation of PS quickly increasing the viscosity. The benefit of the large NPC is to be able to recover from an initial dip (Figure 19 a)) and continue discharging more of the PS in the electrolyte. This implies that the large interparticle pores does indeed enhance the mass transfer for lithium ions to the surface of the reaction sites.

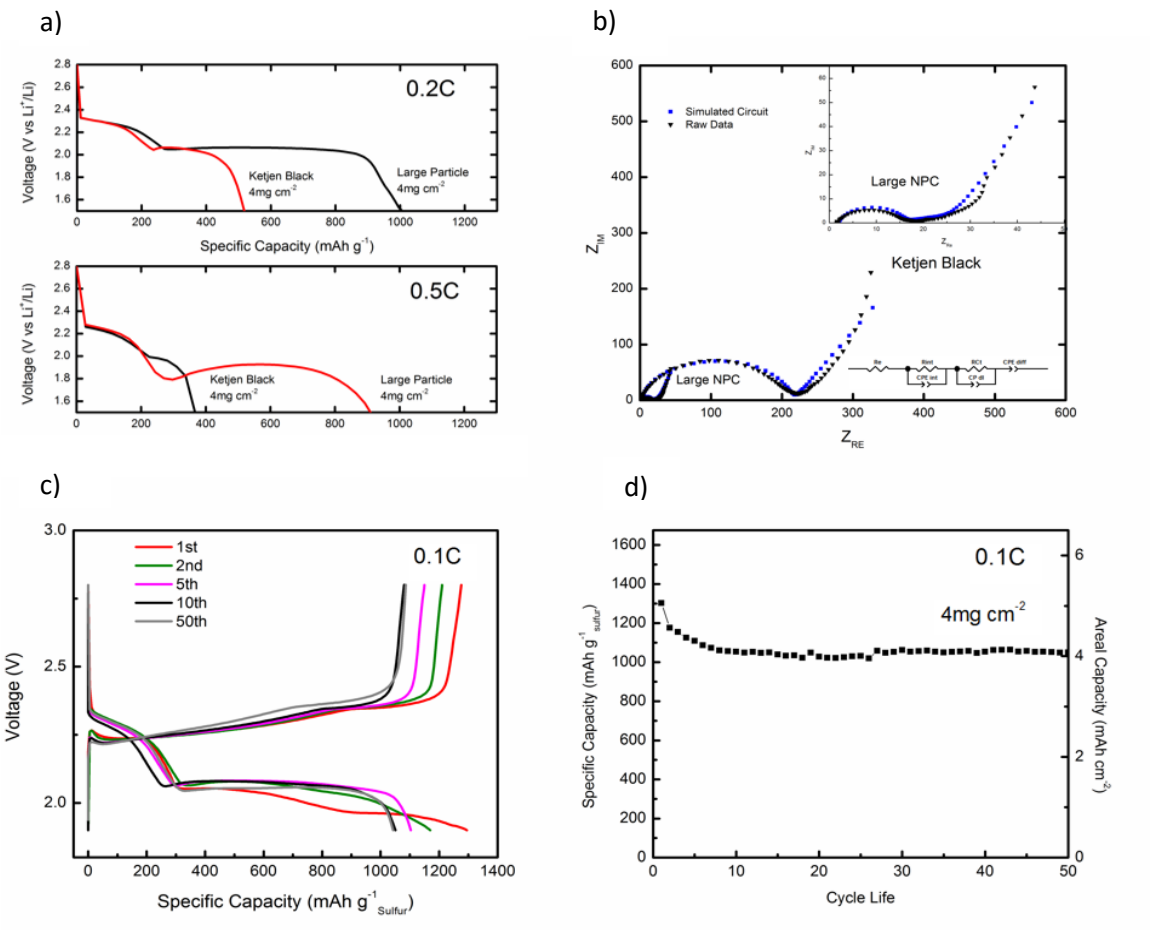

Figure 19: Voltage profile of 4 mg cm^{-2} (a), short cycle life test of 4 mg cm^{-2} (b) both at 01C.

From Figure 19 c), the second plateau of discharge increased as the cycle proceeded. This indicates that the electrode underwent an activation phase. Whether this is the consequence of delayed electrode wetting by electrolyte or redistribution of sulfur into a more favorable manner, the high loading large NPC electrode was able to recover and retain a large majority of its initial discharge capacity. Figure 19 d) depicts the cycle stability performance normalized to S content and also to, more practically, the total electrode area. In comparison to the 400 cycle through which the small NPC particle underwent, 50 cycles appears not exceptional. However, in the case of a high loading electrode, the absolute flux of PS out of the cathode is significantly higher than that of the small NPC. This commonly results in quicker decay of performance. Therefore 50 cycles is indeed quite exceptional and is the result of not only the high surface area, porous network and nitrogen doping but also the drastic increase in pore volume of the large particle

due to the sodium ions. The increase in micropores can effective limit the PS diffusion even at a higher absolute flux. The capacity of the large NPC particle electrode possessed a 1st discharge of more than 1300 mAh g^{-1}_{sulfur} (78% of theoretical, 1675 mAh g^{-1}) and stabilized at ~950 mAh g^{-1}_{sulfur} after 50 cycles at 0.1C. As mentioned in Pope et al's recent review paper [22], the loading has to be around 4-5 mg_{sulfur} cm^{-2} or higher in order to be commercially viable. In this work we have demonstrated a battery with loading 4 mg_{sulfur} cm^{-2} which corresponds to an energy density of about 400 Wh kg^{-1}, with a capacity of 950 mAh g^{-1}_{sulfur} and an average working voltage of 2.1V.

4.4 Section Conclusions and remarks

Mesoporous nitrogen doped carbon was synthesized through a silica templated melamine-formaldehyde resin solution. NaCl was included in the synthesis procedure as a dual purpose chemical additive. First, the added sodium ions adsorbed onto the polymer composite surfaces and reduced the zeta potential. The neutralized surface charge accelerated agglomeration during the polymerization process. This enable the fabrication of a high loading electrode 4mg cm^{-2} of sulfur in addition to decreasing the required binder content to a mere 7.5%. Furthermore, the larger particle containing larger interparticle pores to facilitate lithium ion mass transfer. Secondly, the sodium ions adsorbed onto the polymer composite, imbedded themselves into the carbon precursor matrix and acted as a micropore template. The resulting 4 mg cm-2 electrodes fabricated from our advanced porous carbon material cycled at 0.1C delivered an impressive initial discharge capacity of 1300 mAh g^{-1}_{sulfur} and still maintained 950 mAh g^{-1}_{sulfur} after 50 cycles. More impressively an areal capacity of 4 mAh cm^{-2} was achieved.

5.0 Conclusions of thesis

In thesis, we have developed a nitrogen doped porous carbon by *in situ* polymerization of melamine and formaldehyde with nano-sized silica template. XRD and SEM was used to confirm the complete removal of silica template from the porous carbon. The particles were studied with SEM and revealed to be around 500 nm in diameter with mesopores of ~20 nm in alignment with the size of the silica template used. Furthermore, from BET measurements, the surface area and pore volume was found to be ~500 $m^2 g^{-1}$ and ~1.2 $cm^3 g^{-1}$ respectively. Interestingly the pore size distribution implied that the silica template only represented a small fraction of the pore volume, but instead there exist a large amount of micropores generated from decomposition and evaporation of volatiles from the melamine-formaldehyde carbon precursor. Nitrogen doping was confirmed to be ~15% by mass with the majority in the pyridinic and pyrollic form with XPS. After impregnation of the pores with sulfur, TGA was conducted to determine the exact mass ration of sulfur in the carbon/sulfur composite. Furthermore, XRD revealed that no sharp sulfur peak can be found indicating that the sulfur is in either an amorphous form or nano-sized. SEM revealed there is no large agglomerates of sulfur in the carbon/sulfur composite implying a homogenous distribution of sulfur throughout the porous carbon. The material was able to deliver an impressive 100 cycles with ~81% retention at 0.2C ending with ~860 mAh g^{-1}. Such high utilization of sulfur at 0.2C is an indicate that the broad sulfur XRD peak is not due to a nano-film or nanoparticles within the porous carbon that is electronically assessable by electrons. A large increase in performance compared to Ketjen black was observed which only delivered ~450 mAh g^{-1} at its 100^{th} cycle at 0.2C. To obtain an electrode of sufficiently high sulfur loading a thicker electrode was attempted. The small particle nitrogen-doped porous carbon was unable to form a mechanically stable high loading electrode. At 110 μm or 4mg cm^{-2} the electrode possessed significant cracks and quickly flaked/delaminated from the current collector upon the slightest geometric manipulation of the electrode. This motivated the fabrication of large particle nitrogen doped porous carbon. Through the addition of NaCl early on in the synthesis procedure large agglomerates of nitrogen doped porous carbon was obtained. From TEM analysis, the micron sized

particle appeared to be composed of smaller particles (~500 nm) with light regions in between them. The light regions were reasoned to be additional melamine formaldehyde polymer acting as glue, adhering the whole aggregate together. From DLS and SEM results, the particle size appeared to have shifted drastically from the nanoscale (~500 nm) to the micron scale (2-4 μm). Furthermore, the zeta potential was found to decreased from ~-10mV to ~-1.6 mV upon addition of NaCl possibly indicating that the accelerated aggregation was indeed induced by the addition of NaCl. These large particle nitrogen doped porous carbon was used to fabricated a high loading 110 μm electrode. The quality of the obtained electrode was significantly superior to that of the small particle. Furthermore, this was achieved with only half the binder content and could maintain its mechanical integrity throughout cutting to form the appropriate coin cell geometry. SEM of these electrode revealed that the porosity could be visually confirmed to be greater for the large particle than the small particle. From electrochemical impedance spectroscopy the large particle nitrogen doped porous carbon revealed a significantly lowered impedance values for Rint, Rct and CPEdiff indicating that the mass transfer for the large particle was indeed better. To further corroborate the benefits of a larger particle size, rate performance tests on 4mg cm^{-2} sulfur loading electrodes indicated that the large particle electrode was able to discharge up to 0.5C with a capacity of ~900 mAh g^{-1} whereas the small particle KB electrode was only able to discharge 350 mAh g^{-1} at 0.5C. At a loading of 4 mg cm^{-2} ,the electrode were able to discharge around 1000 mAh g^{-1}_{sulfur} at 0.1C for 50 cycles which corresponds to ~4 mAh cm^{-2}.

6.0 Recommendations and future works

Future work could include the optimization of the salt addition procedure to increase the uniformity of the particles. The cascading size of the particle most likely decreased the porosity of the electrode and reduced rate performance. Since the use of salt is also not required to make larger particle, exploration of other technique such as spray drying could be done to increase the particle size. Although the performance of the NPC was good, more improvements can be made. A 63% retention after 400 cycles can be improved to as high as possible to further increase the lifespan of the battery. If the nitrogen doped porous carbon platform is to be kept, then possible optimization of carbonization temperature and time could be made to achieve as high of a pyridinic and pyrollic form of nitrogen doping as possible. Furthermore, a different template can be used to replace silica, this will address the safety concerns associated with the chemicals required to etch the silica. Currently silica will require either hot concentrated NaOH or HF, both of which are extremely dangerous.

Finally, it is naïve to claim that a sufficiently high loading LIS will immediately warrant commercialization. Loading is only one parameter of concern for realizing this or any battery for commercial application. Other factors such as cell design, electrolyte-to-sulfur ratio, rate performance, storage life, cost of synthesis, and the material must be optimized in relation to each other before any commercialization can be made. Therefore future work could be focussed on optimizing not only the loading and emulated performance tests, but also all the other factors related to large scale manufacturing and real end-user performance. One such method would be to fabricate cylindrical or pouch cell type batteries to test the LIS instead of “idealized” coin cells.

Reference

[1] J. K. Park, "Introduction," in *Principles and Applications of Lithium Secondary Batteries*, ed Germany: Wiley-VCH, 2012, pp. 1-4.

[2] B. C. H. Steele, "Chemical Diffusion," *Fast ion Transport in Solids*, 1973.

[3] A. Fotouhi, D. J. Auger, K. Propp, S. Longo, and M. Wild, "A review on electric vehicle battery modelling: From Lithium-ion toward Lithium–Sulphur," *Renewable and Sustainable Energy Reviews*, vol. 56, pp. 1008-1021, 2016.

[4] L. O. N. M. Wild , T. Zhang , R. Purkayastha , G. Minton , M. Marinescu and G. J. Offer, "Lithium sulfur batteries, a mechanistic review," *Energy Environ. Science*, October 7th 2015 2015.

[5] A. G. Ritchie, C. O. Giwa, J. C. Lee, P. Bowles, A. Gilmour, J. Allan, D. A. Rice, F. Brady, and S. C. E. Tsang, "Future cathode materials for lithium rechargeable batteries," *Journal of Power Sources*, vol. 80, pp. 98-102, Jul-Aug 1999.

[6] "A Lithium/Dissolved Sulfur Battery with an Organic Electrolyte."

[7] C. Barchasz, F. Molton, C. Duboc, J. C. Lepretre, S. Patoux, and F. Alloin, "Lithium/sulfur cell discharge mechanism: an original approach for intermediate species identification," *Anal Chem*, vol. 84, pp. 3973-80, May 1 2012.

[8] X. Ji and L. F. Nazar, "Advances in Li–S batteries," *Journal of Materials Chemistry*, vol. 20, p. 9821, 2010.

[9] H. L. Wang, Y. Yang, Y. Y. Liang, J. T. Robinson, Y. G. Li, A. Jackson, Y. Cui, and H. J. Dai, "Graphene-Wrapped Sulfur Particles as a Rechargeable Lithium-Sulfur Battery Cathode Material with High Capacity and Cycling Stability," *Nano Lett*, vol. 11, pp. 2644-2647, Jul 2011.

[10] X. L. Ji, K. T. Lee, and L. F. Nazar, "A highly ordered nanostructured carbon-sulphur cathode for lithium-sulphur batteries," *Nature Materials*, vol. 8, pp. 500-506, Jun 2009.

[11] J. Balach, T. Jaumann, M. Klose, S. Oswald, J. Eckert, and L. Giebeler, "Functional Mesoporous Carbon-Coated Separator for Long-Life, High-Energy Lithium-Sulfur Batteries," *Advanced Functional Materials*, vol. 25, pp. 5285-5291, 2015.

[12] S. N. L. Wook Ahn, Dong Un Lee, Kwang-Bum Kim, Zhongwei Chen and a. S.-H. Yeon, "Interaction mechanism between a functionalized protective layer and dissolved polysulfide for extended cycle life of lithium sulfur batteries," *Journal of Materials Chemistry A*, vol. 2015, p. 9461, 2015.

[13] M. Agostini, S. Xiong, A. Matic, and J. Hassoun, "Polysulfide-containing Glyme-based Electrolytes for Lithium Sulfur Battery," *Chemistry of Materials*, vol. 27, pp. 4604-4611, 2015.

[14] F. Wu, J. T. Lee, N. Nitta, H. Kim, O. Borodin, and G. Yushin, "Lithium iodide as a promising electrolyte additive for lithium-sulfur batteries: mechanisms of performance enhancement," *Adv Mater*, vol. 27, pp. 101-8, Jan 7 2015.

[15] W. Ahn, M. H. Seo, Y. S. Jun, D. U. Lee, F. M. Hassan, X. Wang, A. Yu, and Z. Chen, "Sulfur nano-granular film coated three-dimensional graphene sponge based high power lithium sulfur battery," *ACS Appl Mater Interfaces,* Jan 8 2016.

[16] G. Zhou, E. Paek, G. S. Hwang, and A. Manthiram, "Long-life Li/polysulphide batteries with high sulphur loading enabled by lightweight three-dimensional nitrogen/sulphur-codoped graphene sponge," *Nat Commun,* vol. 6, 2015.

[17] J. Guo, Y. Xu, and C. Wang, "Sulfur-impregnated disordered carbon nanotubes cathode for lithium-sulfur batteries," *Nano Lett,* vol. 11, pp. 4288-94, Oct 12 2011.

[18] K. T. L. a. L. F. N. Xiulei Ji, "A highly ordered nanostructured carbon–sulphur cathode for lithium–sulphur batteries," *Nature Materials,* vol. 8, 2009.

[19] N. Jayaprakash, J. Shen, S. S. Moganty, A. Corona, and L. A. Archer, "Porous hollow carbon@sulfur composites for high-power lithium-sulfur batteries," *Angew Chem Int Ed Engl,* vol. 50, pp. 5904-8, Jun 20 2011.

[20] J. Song, T. Xu, M. L. Gordin, P. Zhu, D. Lv, Y.-B. Jiang, Y. Chen, Y. Duan, and D. Wang, "Nitrogen-Doped Mesoporous Carbon Promoted Chemical Adsorption of Sulfur and Fabrication of High-Areal-Capacity Sulfur Cathode with Exceptional Cycling Stability for Lithium-Sulfur Batteries," *Advanced Functional Materials,* vol. 24, pp. 1243-1250, 2014.

[21] J. Song, M. L. Gordin, T. Xu, S. Chen, Z. Yu, H. Sohn, J. Lu, Y. Ren, Y. Duan, and D. Wang, "Strong lithium polysulfide chemisorption on electroactive sites of nitrogen-doped carbon composites for high-performance lithium-sulfur battery cathodes," *Angew Chem Int Ed Engl,* vol. 54, pp. 4325-9, Mar 27 2015.

[22] M. A. Pope and I. A. Aksay, "Structural Design of Cathodes for Li-S Batteries," *Advanced Energy Materials,* vol. 5, pp. n/a-n/a, 2015.

[23] J. Xiao, "Understanding the Lithium Sulfur Battery System at Relevant Scales," *Advanced Energy Materials,* vol. 5, pp. n/a-n/a, 2015.

[24] D. Lv, J. Zheng, Q. Li, X. Xie, S. Ferrara, Z. Nie, L. B. Mehdi, N. D. Browning, J.-G. Zhang, G. L. Graff, J. Liu, and J. Xiao, "High Energy Density Lithium-Sulfur Batteries: Challenges of Thick Sulfur Cathodes," *Advanced Energy Materials,* vol. 5, pp. n/a-n/a, 2015.

[25] R. Yi, S. Chen, J. Song, M. L. Gordin, A. Manivannan, and D. Wang, "High-Performance Hybrid Supercapacitor Enabled by a High-Rate Si-based Anode," *Advanced Functional Materials,* vol. 24, pp. 7433-7439, 2014.

[26] T. Xu, J. Song, M. L. Gordin, H. Sohn, Z. Yu, S. Chen, and D. Wang, "Mesoporous carbon-carbon nanotube-sulfur composite microspheres for high-areal-capacity lithium-sulfur battery cathodes," *ACS Appl Mater Interfaces,* vol. 5, pp. 11355-62, Nov 13 2013.

[27] J. L. Lina Wang , Shouyi Yuan , Yonggang Wang and Yongyao Xia "To mitigate self-discharge of lithium–sulfur batteries by optimizing ionic liquid electrolytes," *Energy Environ. Science,* vol. 2016, November 13th 2015 2016.

[28] X. Qian, L. Jin, D. Zhao, X. Yang, S. Wang, X. Shen, D. Rao, S. Yao, Y. Zhou, and X. Xi, "Ketjen Black-MnO Composite Coated Separator For High Performance Rechargeable Lithium-Sulfur Battery," *Electrochimica Acta,* vol. 192, pp. 346-356, 2016.

[29] K. B. Singh and M. S. Tirumkudulu, "Cracking in drying colloidal films," *Phys Rev Lett,* vol. 98, p. 218302, May 25 2007.

[30] Z. Deng, Z. Zhang, Y. Lai, J. Liu, J. Li, and Y. Liu, "Electrochemical Impedance Spectroscopy Study of a Lithium/Sulfur Battery: Modeling and Analysis of Capacity Fading," *Journal of the Electrochemical Society,* vol. 160, pp. A553-A558, 2013.

[31] L. Yuan, X. Qiu, L. Chen, and W. Zhu, "New insight into the discharge process of sulfur cathode by electrochemical impedance spectroscopy," *Journal of Power Sources,* vol. 189, pp. 127-132, 2009.

[32] N. A. Cañas, K. Hirose, B. Pascucci, N. Wagner, K. A. Friedrich, and R. Hiesgen, "Investigations of lithium–sulfur batteries using electrochemical impedance spectroscopy," *Electrochimica Acta,* vol. 97, pp. 42-51, 2013.

[33] L. F. Nazar and Q. Pang, "Long-Life and High Areal Capacity Li-S Batteries Enabled by a Light-Weight Polar Host with Intrinsic Polysulfide Adsorption," *ACS Nano,* Feb 3 2016.

[34] Q. Pang, J. Tang, H. Huang, X. Liang, C. Hart, K. C. Tam, and L. F. Nazar, "A Nitrogen and Sulfur Dual-Doped Carbon Derived from Polyrhodanine@Cellulose for Advanced Lithium-Sulfur Batteries," *Adv Mater,* vol. 27, pp. 6021-8, Oct 2015.

[35] H. Nie, H. Zhang, Y. Zhang, T. Liu, J. Li, and Q. Lai, "Nitrogen enriched mesoporous carbon as a high capacity cathode in lithium-oxygen batteries," *Nanoscale,* vol. 5, pp. 8484-7, Sep 21 2013.

[36] D. J. Merline, S. Vukusic, and A. A. Abdala, "Melamine formaldehyde: curing studies and reaction mechanism," *Polymer Journal,* vol. 45, pp. 413-419, 2012.

[37] S. S. Zhang, "Role of LiNO3 in rechargeable lithium/sulfur battery," *Electrochimica Acta,* vol. 70, pp. 344-348, 2012.

[38] M. Ghavidel and E. Easton, "Improving the Ethanol Oxidation Activity of Pt-Mn Alloys through the Use of Additives during Deposition," *Catalysts,* vol. 5, pp. 1016-1033, 2015.

[39] W. Zhou, C. Wang, Q. Zhang, H. D. Abruña, Y. He, J. Wang, S. X. Mao, and X. Xiao, "Tailoring Pore Size of Nitrogen-Doped Hollow Carbon Nanospheres for Confining Sulfur in Lithium-Sulfur Batteries," *Advanced Energy Materials,* vol. 5, pp. n/a-n/a, 2015.

[40] S. Hou, X. Cai, H. Wu, X. Yu, M. Peng, K. Yan, and D. Zou, "Nitrogen-doped graphene for dye-sensitized solar cells and the role of nitrogen states in triiodide reduction," *Energy & Environmental Science,* vol. 6, p. 3356, 2013.

[41] L. Sun, L. Wang, C. G. Tian, T. X. Tan, Y. Xie, K. Y. Shi, M. T. Li, and H. G. Fu, "Nitrogen-doped graphene with high nitrogen level via a one-step hydrothermal reaction

of graphene oxide with urea for superior capacitive energy storage," *RSC Advances*, vol. 2, pp. 4498-4506, 2012.

[42] W. H. Shin, H. M. Jeong, B. G. Kim, J. K. Kang, and J. W. Choi, "Nitrogen-doped multiwall carbon nanotubes for lithium storage with extremely high capacity," *Nano Lett,* vol. 12, pp. 2283-8, May 9 2012.

[43] H. B. Wang, T. Maiyalagan, and X. Wang, "Review on Recent Progress in Nitrogen-Doped Graphene: Synthesis, Characterization, and Its Potential Applications," *Acs Catalysis,* vol. 2, pp. 781-794, May 2012.

[44] L.-B. Xing, K. Xi, Q. Li, Z. Su, C. Lai, X. Zhao, and R. V. Kumar, "Nitrogen, sulfur-codoped graphene sponge as electroactive carbon interlayer for high-energy and -power lithium–sulfur batteries," *Journal of Power Sources,* vol. 303, pp. 22-28, 2016.

[45] F. Wu, Y. Ye, R. Chen, J. Qian, T. Zhao, L. Li, and W. Li, "Systematic Effect for an Ultralong Cycle Lithium-Sulfur Battery," *Nano Lett,* vol. 15, pp. 7431-9, Nov 11 2015.

[46] X. G. Sun, X. Wang, R. T. Mayes, and S. Dai, "Lithium-sulfur batteries based on nitrogen-doped carbon and an ionic-liquid electrolyte," *ChemSusChem,* vol. 5, pp. 2079-85, Oct 2012.

[47] M. Wang, Y. Zhang, H. Zhang, and H. Zhang, "A Microsized Cagelike Sulfur/Carbon Composite for a Lithium/Sulfur Battery with Excellent Performance," *ChemPlusChem,* vol. 79, pp. 919-924, 2014.

[48] P. Bhattacharya, M. I. Nandasiri, D. Lv, A. M. Schwarz, J. T. Darsell, W. A. Henderson, D. A. Tomalia, J. Liu, J.-G. Zhang, and J. Xiao, "Polyamidoamine dendrimer-based binders for high-loading lithium–sulfur battery cathodes," *Nano Energy,* vol. 19, pp. 176-186, 2016.

[49] B. He, W. C. Li, C. Yang, S. Q. Wang, and A. H. Lu, "Incorporating Sulfur Inside the Pores of Carbons for Advanced Lithium-Sulfur Batteries: An Electrolysis Approach," *ACS Nano,* Jan 8 2016.

[50] Y. Wu, Y. Li, L. Qin, F. Yang, and D. Wu, "Monodispersed or narrow-dispersed melamine–formaldehyde resin polymer colloidal spheres: preparation, size-control, modification, bioconjugation and particle formation mechanism," *J. Mater. Chem. B,* vol. 1, pp. 204-212, 2013.

[51] K. L. N. C. R. O. UEK, "Particle size control in dispersion polymerization of polystyrene," *Can. J. Chem.* , vol. 63, 1984.

[52] E. D. S. S. SHEN, and M. S. EL-AASSER, "Control of Particle Size in Dispersion Polymerization of Methyl Methacrylate," *Journal of Polymer Science: Part A: Polymer Chemistry,* vol. 31, 1993.

[53] J. Liu, S. Z. Qiao, H. Liu, J. Chen, A. Orpe, D. Zhao, and G. Q. Lu, "Extension of the Stober method to the preparation of monodisperse resorcinol-formaldehyde resin polymer and carbon spheres," *Angew Chem Int Ed Engl,* vol. 50, pp. 5947-51, Jun 20 2011.

[54] H. Zheng, G. Zhu, S. Jiang, T. Tshukudu, X. Xiang, P. Zhang, and Q. He, "Investigations of coagulation–flocculation process by performance optimization, model prediction and fractal structure of flocs," *Desalination,* vol. 269, pp. 148-156, 2011.

[55] K. W. H. Nakagawa, Y. Harada, K. Miura "Control of micropore formation in the carbonized ion exchange resin by utilizing pillar effect," *Carbon,* vol. 37, 1999.

[56] A. B. Deon Hines, and Teresa J. Bandosz "Surface Properties of Porous Carbon Obtained from Polystyrene Sulfonic Acid-Based Organic Salts," *Langmuir,* vol. 20, 2004.

[57] J. Ming, Y. Wu, G. Liang, J.-B. Park, F. Zhao, and Y.-K. Sun, "Sodium salt effect on hydrothermal carbonization of biomass: a catalyst for carbon-based nanostructured materials for lithium-ion battery applications," *Green Chemistry,* vol. 15, p. 2722, 2013.

[58] C. S. A. Schneider, H. Sommer, J. Janek and T. Brezesinski, "Free-standing and binder-free highly N-doped carbon/sulfur cathodes with tailorable loading for high-areal-capacity lithium–sulfur batteries," *Journal of Materials Chemistry A,* vol. 2015, p. 20482, 2015.

[59] Y. Liu, J. Guo, J. Zhang, Q. Su, and G. Du, "Graphene-wrapped sulfur nanospheres with ultra-high sulfur loading for high energy density lithium–sulfur batteries," *Applied Surface Science,* vol. 324, pp. 399-404, 2015.

[60] J. Yan, X. Liu, H. Qi, W. Li, Y. Zhou, M. Yao, and B. Li, "High-Performance Lithium–Sulfur Batteries with a Cost-Effective Carbon Paper Electrode and High Sulfur-Loading," *Chemistry of Materials,* vol. 27, pp. 6394-6401, 2015.

Appendix

Appendix A: calculation of specific lithium capacity of cobalt oxide and sulfur

Let specific lithium capacity =SLC:

$$SLC = \frac{(Total\ charge\ of\ lithium\ stored)}{Mass\ of\ lithium\ storage\ medium}$$

In the case of CoO_2 the lithiation reaction is as follows:

$$Li^+ + CoO_2 + e^{-1} = LiCoO_2$$

For every mole of cobalt oxide one mole of lithium ion is stored:

$$(Total\ charge\ of\ lithium\ stored) = 1mole_{Li} * \frac{1mole_{electron}}{1mole_{Li}} * \frac{6.02X10^{23}(\#of\ electrons)}{mole_{electron}} * \frac{1.602X10^{-19}Coulombs}{\#of\ electrons}$$

This would yield:

$$(Total\ charge\ of\ lithium\ stored) = 96440\ Coulombs$$

Unit conversion is required to obtain a more conventional unit, i.e. mAh:

$$(Total\ charge\ of\ lithium\ stored) = 96440\ A\left(\frac{C}{seconds}\right) * t(seconds) * 1000\frac{mA}{A} * \frac{h}{3600\ seconds} = 26789\ mAh$$

Mass of lithium storage medium can be calculated by the following equation:

$$Mass\ of\ lithium\ storage\ medium = Molar\ mass * Moles\ of\ lithium\ storage\ medium$$

$$Mass\ of\ lithium\ storage\ medium = 1mole * 91\frac{g}{mole} = 75g$$

Substituting all variables:

$$SLC = \frac{(Total\ charge\ of\ lithium)}{Mass\ of\ lithium\ storage\ medium} = \frac{26780mAh}{91g} = 294mAh\ /g$$

Similarly for sulfur:

$$SLC = \frac{(Total\ charge\ of\ lithium)}{Mass\ of\ lithium\ storage\ medium} = \frac{53578mAh}{32g} = 1675mAh\ /g$$

For calculation of energy, a full cell configuration is usually considered:

In the case of a typical LIB the anode is graphite which bonds the lithium the following manner:

$$Li^{+} + C_6 + e^{-1} = LiC_6$$

$$SLC = \frac{(Total\ charge\ of\ lithium)}{Mass\ of\ lithium\ storage\ medium} = \frac{26780mAh}{12 * 6g} = 372mAh\ /g$$

A full cell would have a specific capacity for lithium of:

$$SLC = \frac{372mAh}{1g + \frac{372}{294} * 1g} = \ 164\ mAh/g$$

At an operating voltage of 3.7V:

$$Theoretical\ Energy\ Density = 607.6\ Wh/kg$$

Not including the different battery components.

Similarly for a LIS battery with a lithium anode and sulfur cathode:

A full cell would have a specific capacity for lithium of:

$$SLC = \frac{53578mAh}{32g + 14g} = \ 1164\ mAh/g$$

At an operating voltage of 2.1V:

$$Theoretical\ Energy\ Density = 2500\ Wh/kg$$

Appendix B: SEM of drop casted large and small NPC particles: